Copyright

by

Logan Brien Tussey

2015

The Thesis Committee for Logan Brien Tussey
Certifies that this is the approved version of the following thesis:

Depositional environment, sequence stratigraphy, and reservoir quality of the Tonkawa Sandstone in the western Anadarko Basin, Hemphill, Lipscomb and Roberts Counties, Texas

APPROVED BY
SUPERVISING COMMITTEE:

Supervisor: _____
William L. Fisher

Co-Supervisor: _____
William A. Ambrose

_____
Bruce L. Cutright

Depositional environment, sequence stratigraphy, and reservoir quality of the Tonkawa Sandstone in the western Anadarko Basin, Hemphill, Lipscomb and Roberts Counties, Texas

by

Logan Brien Tussey, B.S.

Thesis

Presented to the Faculty of the Graduate School of

The University of Texas at Austin

in Partial Fulfillment

of the Requirements

for the Degree of

Master of Science in Energy and Earth Resources

The University of Texas at Austin

May 2015

Acknowledgments

I would first like to thank my thesis committee, Dr. William Fisher, William Ambrose, and Bruce Cutright for their steadfast guidance and support during my time at the University of Texas at Austin. Thank you to my mentors on the STARR Project: Tucker Hentz for his expertise in Pennsylvanian stratigraphy, Dr. Shirley Dutton and Dr. Gregory Frebourg for their assistance with petrographic analysis, and Shadiyat Bello for her guidance with the software program Petra. I would also like to thank James Donnelly, Nathan Ivicic, and all the staff at the Core Research Center for their help with core samples. Finally, thank you to my friends and family whose love and support has always been with me, in all of my pursuits.

Abstract

Depositional environment, sequence stratigraphy, and reservoir quality of the Tonkawa Sandstone in the western Anadarko Basin, Hemphill, Lipscomb and Roberts Counties, Texas

Logan Brien Tussey, M.S.E.E.R.

The University of Texas at Austin, 2015

Supervisors: William L. Fisher and William A. Ambrose

The Anadarko Basin contains some of the most prolific hydrocarbon reserves in all of North America. A recent USGS publication estimated undiscovered resources across the basin to be 495 million barrels of oil (MMBO), 27 trillion cubic feet of natural gas (TCFG), and 410 million barrels of natural gas liquids (MMBNGL). Pennsylvanian-age sandstones contribute substantially to total estimated reserves within the basin. The focus of this study is the late Pennsylvanian Tonkawa Sandstone, the lowermost unit of the Douglas Group, Virgilian Series. Through the integration of core analysis, subsurface mapping, petrographic analysis, and porosity and permeability data, this study presents a detailed analysis of the Tonkawa Sandstone across approximately 1,400 mi^2 (3,630 km^2) in the western Anadarko Basin.

The Tonkawa Sandstone is comprised of three high-order transgressive-regressive sequences within one larger, lower-order sequence. Sandstone-body distribution varies greatly, depending upon depositional environments and their associated facies. The Tonkawa Sandstone was deposited in deltaic and estuarine environments with a source area to the northeast. The

HST-2 interval, the oldest sandstone-rich sequence in the Tonkawa Sandstone, was deposited in a deltaic environment with a mixed wave and tide-dominated energy regime. The younger HST-3 interval was deposited in a tide-dominated deltaic environment. The youngest interval, TST-3, was deposited in a mixed wave and tide-dominated transgressive estuarine environment. The Tonkawa Sandstone is a sublitharenite to litharenite. Widespread quartz overgrowths minimize variation in reservoir quality among facies. However, more proximal facies display better reservoir quality. Detailed characterization of Pennsylvanian formations such as the Tonkawa Sandstone contributes greatly to the understanding of similar formations within the Anadarko Basin, and other foreland and cratonic basins worldwide.

Table of Contents

List of Tables

List of Figures

Chapter 1: Introduction

The Tonkawa Sandstone, a Pennsylvanian-age formation in the Anadarko Basin, represents the lowermost unit of the Douglas Group of the Virgilian Series (Figure 1). The Tonkawa Sandstone produces oil and gas in Oklahoma and the Texas Panhandle. Characterization of productive formations such as the Tonkawa Sandstone yields a better understanding of other Pennsylvanian stratigraphic units, thus increasing total hydrocarbon recovery in the Anadarko Basin.

Current research on the western shelf of the Anadarko Basin is relatively limited, despite decades of hydrocarbon explorations and production. The Tonkawa Sandstone, like many other formations in the Anadarko Basin, has been interpreted as having been deposited in a variety of depositional environments, including submarine fan (Kumar and Slatt, 1984), fluvial-dominated deltaic (Andrews, 1997), and mixed fluvial and tide-modified estuarine (Cashman, 2011). Thus far the bulk of research on the Tonkawa Sandstone has been focused in Oklahoma. Limited data exists concerning depositional environment interpretations for the Tonkawa Sandstone in the western Anadarko Basin, in Texas.

WESTERN ANADARKO BASIN			
SYSTEM	SERIES	GROUP	FORMATION
PERMIAN	GUADALUPIAN	WHITEHORSE	QUARTERMASTER
			ALIBATES DOLOMITE
		NIPPEWALLA	SAN ANDRES GLORIETA SS. AT BASE
	LEONARDIAN		CLEAR FORK (INCLUDES CIMMARON ANHY. AND "TUBB ZONE")
		SUMNER	WICHITA ("PANHANDLE LIME")
	WOLFCAMPIAN	CHASE	HERINGTON OR "BROWN DOLOMITE" AT TOP
		COUNCIL GROVE	
		ADMIRE	
PENNSYLVANIAN	VIRGILIAN	WABUNSEE	
		SHAWNEE	TOPEKA LS. AT TOP OREAD LS AT BASE
		DOUGLAS	TONKAWA SS. AT BASE
	MISSOURIAN	PEDEE	
		LANSING	
		KANSAS CITY	
		PLEASANTON	
	DESMOINESIAN	MARMATON	OSWEGO LS. AT BASE
		CHEROKEE	
	ATOKANAN		13 FINGER LS. AT BASE
	MORROWAN	UPPER	KEYES SD. AT BASE (RESTRICTED)
		LOWER	
	SPRINGERIAN		

Figure 1: Texas Panhandle stratigraphy (modified from Cunningham, 1961).

Through the integration of core analysis, subsurface mapping, petrographic analysis, and porosity and permeability data, the objectives of this study are: (1) interpret depositional environments and associated facies for the Tonkawa Sandstone in the western Anadarko Basin; (2) document variations in mineralogy, porosity, and permeability within each facies; (3) construct a sequence stratigraphic framework, and (4) infer sediment source areas.

Study Area

The study area encompasses approximately 1,400 mi^2 (3,630 km^2) and includes all of Hemphill County, southern Lipscomb County, and eastern Roberts County in the Texas Panhandle. The study area was selected because (1) depositional trends for the Tonkawa Sandstone within the western Anadarko Basin were relatively unstudied, (2) the study area is large enough to observe facies variations and depositional trends, (3) core data was available to support depositional environment interpretations, and (4) abundant well control exists.

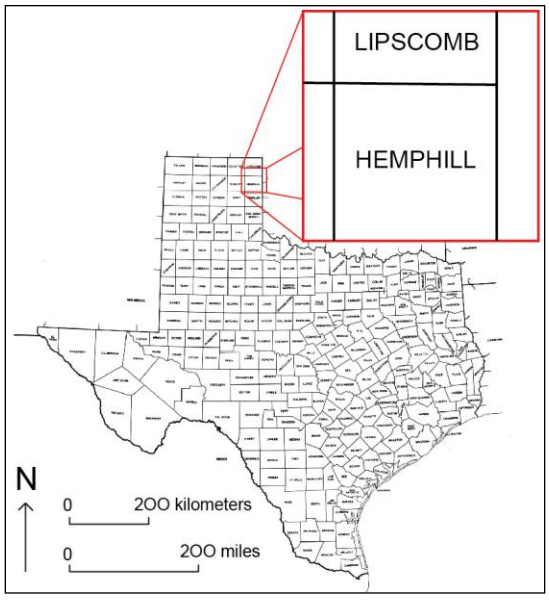

Figure 2: Study area: encompasses ~1,400 mi^2 (3,630 km^2), including all of Hemphill County, southern Lipscomb County, and eastern Roberts County

Regional Geologic History

During Pennsylvanian time, the Anadarko Basin was an area of rapid tectonic subsidence. Deposits within the basin, such as the Tonkawa Sandstone are considered the product of a tectonically-controlled marine advance which resulted in the deposition of "blanket sandstones" across the basin (Rascoe, 1962). "Blanket sandstones" such as the Tonkawa were deposited during periods of regression, within an overall deepening basin (Figure 3). Thick sedimentary deposits that began to fill the deepening basin were sourced from numerous tectonic uplifts (Moore, 1979). Sources of sedimentation during the Pennsylvanian include the Amarillo-Wichita Uplift, the Nemeha Uplift, the Ozark Uplift, the Arbuckle Uplift, as well as other smaller-scale structurally high areas. A tectonically-stable shelf, known as the Central Kansas Platform or Kansas Shelf, was north of the Anadarko Basin (Figure 4). The Kansas Shelf evolved from a low-lying source area and was defined by cyclic carbonate sedimentation in the absence of clastic sedimentation (Moore, 1979).

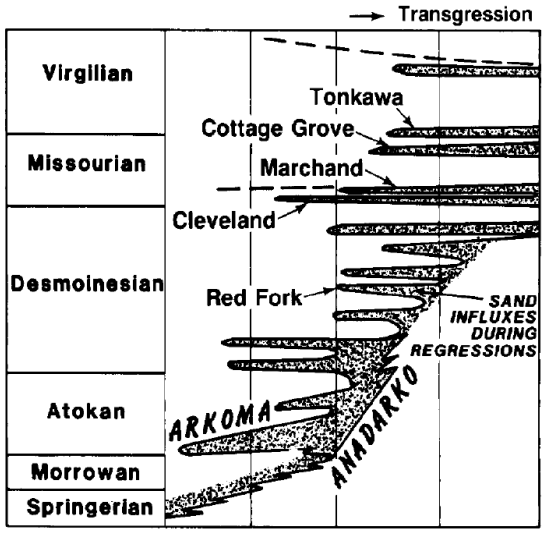

Figure 3: Sand influx during periods of regression within the Anadarko Basin (Kumar and Slatt, 1984)

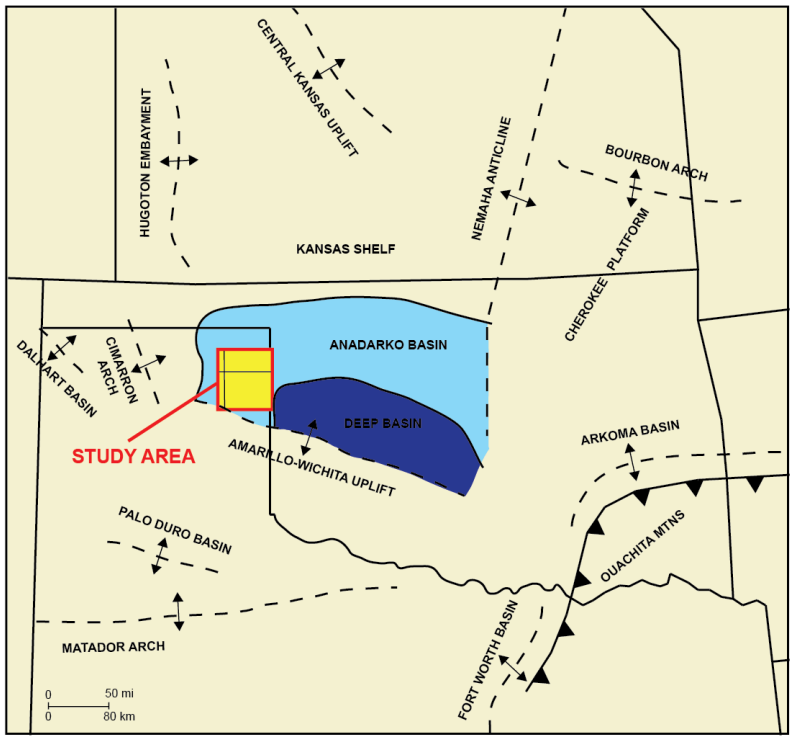

Figure 4: Late Pennsylvanian Basin Configuration and study area

During the Desmoinesian Epoch, sediments were transported into the basin from the Ozark Uplift to the east. Then, throughout the Missourian Epoch the Ouachita Uplift began to serve as the principal source of sediment to the basin until the early to middle Virgilian. Beginning in the middle Pennsylvanian, the Amarillo-Wichita Uplift became a major supplier of sediment to the basin and continued to do so until the Permian (Fies, 1988; Cashman, 2011). It was not until the early Virgilian that fine-grained clastics prograded from the east across Oklahoma to the western extent of the Anadarko Basin. These fine-grained clastics graded into arkosic clastics shed from the Amarillo-Wichita Uplift (Rascoe, 1962), and interfingered with clastics that prograded across the Kansas shelf to the north (Moore, 1979).

Previous Work

Previous work on the Tonkawa Sandstone focused on the eastern portion of the Anadarko Basin, primarily in present day Oklahoma. The Tonkawa Sandstone was named for the Tonkawa Field in Kay County, Oklahoma where petroleum was first produced from anticlinal traps (Clark and Aurin, 1924). The Tonkawa sandstone was first informally subdivided into four members, or "bars" in a study of the Laverne district, an area of Oklahoma that encompasses northwest Beaver County and southeast Stockholm County, Oklahoma (Pate, 1959). Later studies by Pate (1963) separated the Tonkawa into three distinct members separated by intervening shales (Cashman, 2011), which then became the convention for subsurface mapping of the Tonkawa.

Depositional environment interpretations for the Tonkawa Sandstone vary greatly, from deltaic (Khaiwka, 1968) (Padgett, 1988), to deepwater (Kumar and Slatt, 1984) (Billingsley and Draves, 1988), to estuarine (Cashman, 2011). Deepwater interpretations made by Kumar and Slatt (1984) were based primarily on sedimentary structures observed in core, as well from

subsurface mapping. Their study suggested a shelf-to-basin transition for the Tonkawa, utilizing the "three-member" lithostratigraphic correlations established by Pate (1963). The basal member was interpreted as a submarine fan deposit, whereas the middle member was interpreted to be a continental slope deposit, and the upper member was interpreted as shallow-marine in origin. This stratigraphic succession suggests that within the eastern portion of the Anadarko Basin, the Tonkawa was deposited during a period of regression within a larger-scale, tectonically-controlled transgression which the basin was undergoing during the Pennsylvanian.

Kumar and Slatt (1984) primarily focused on descriptions of the informally named middle and lower Tonkawa Sandstone. These authors also recognized a "two-phase depositional sequence" for the middle and lower Tonkawa Sandstone deposited on the slope and basin floor, respectively. During "Phase 1," deposition was interpreted to have occurred within a basin with a relatively steep slope. Shallow-marine clastics were transported across the Kansas Shelf through submarine canyons that formed submarine fans that gradually began to fill the basin. With the gradual filling of the basin, "Phase 2" Tonkawa deposition was characterized by a decrease in slope gradient, with shallower water and shallower channels. The Lower Tonkawa and middle Tonkawa have been interpreted as having been deposited in "Phase 1" and "Phase 2," respectively (Figure 5).

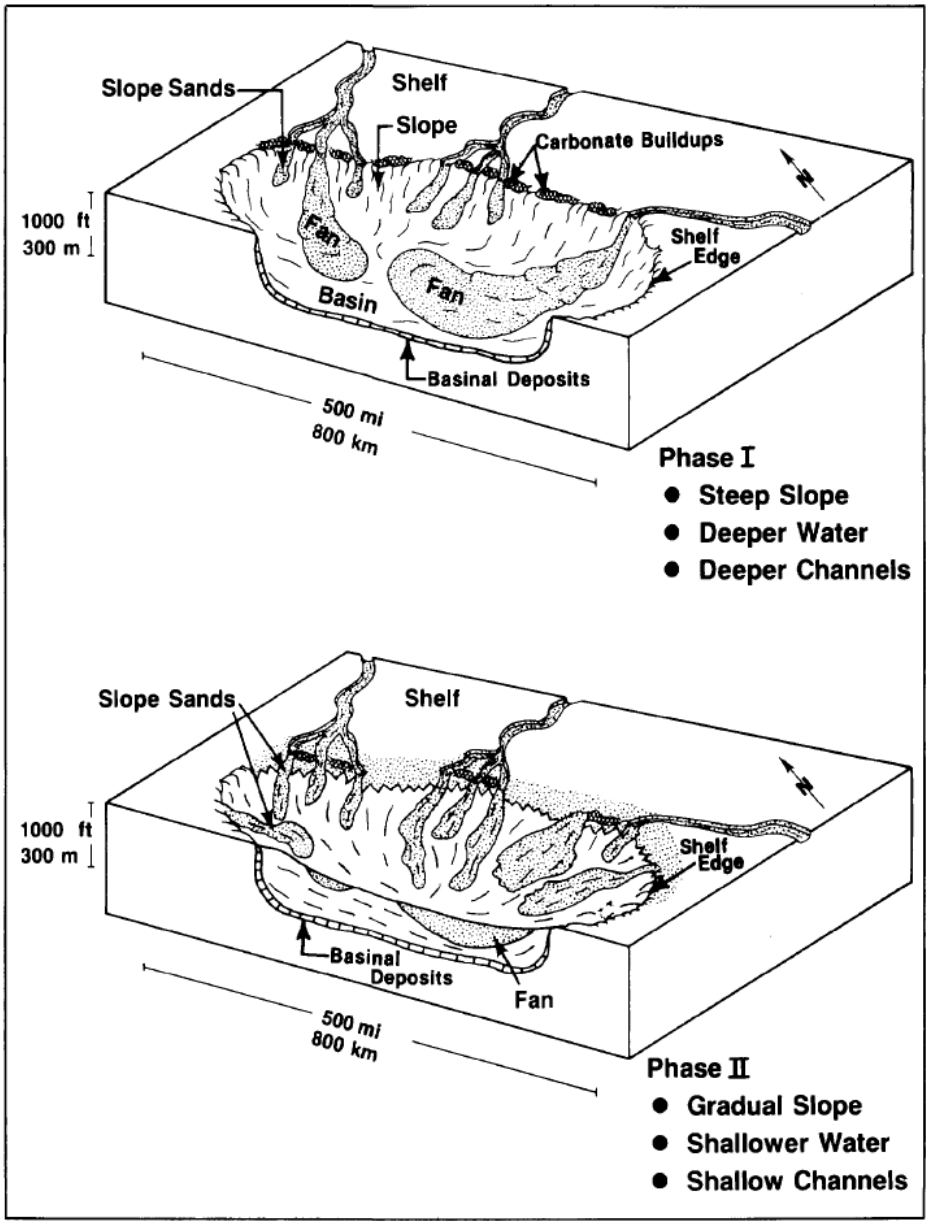

Figure 5: Two-Phase Depositional Sequence for the Tonkawa Sandstone on the basin floor and slope (Kumar and Slatt, 1984).

A deepwater interpretation was also employed by Billingsley and Draves (1988) for a study of Bechthold and Frass fields in Lipscomb County, Texas. This study relied primarily on wireline-log analysis and petrography and employed the "Two-Phase Depositional Sequence"

model, as well as the "three-member" lithostratigraphic correlation established by Kumar and Slatt (1984). Billingsley and Draves (1988) interpreted Tonkawa sandstone bodies to be strike-elongate in a northeast-southwest orientation, extending for tens of miles in length and approximately one mile in width, reworked by offshore currents. This study suggested that additional elongate Tonkawa sandstone bodies may exist further downdip, occurring along strike in a northeast-southwest orientation.

Deltaic and estuarine depositional environments were suggested by Cashman (2011). This study focused on the Tonkawa in northwest Oklahoma and employed the integration of core analysis and wireline log analysis. Based primarily on sedimentary structures observed in core, Cashman (2011) concluded that the Tonkawa was deposited in a deltaic environment influenced by both fluvial and tidal forces, as well as in an estuarine environment during periods of transgression. While this study incorporated a great deal of robust analysis of sedimentary structures in Tonkawa cores, maps were not provided to support environmental interpretations.

The source of sedimentation for the Tonkawa is highly debated. During Tonkawa deposition, it has been suggested that coarse clastics shed from the Amarillo-Wichita Uplift were deposited proximal to the source, whereas finer-grained sediments were only able to prograde relatively short distances before reaching the rapidly deepening western Anadarko Basin (Moore, 1979). Early Virgilian sediments such as the Tonkawa have also been thought to have an eastern source area (Moore, 1979) (Rascoe, 1962). The Ouachita Uplift to the southeast has been suggested (Kumar and Slatt, 1984) as well as a source to the northeast, related to the Tonkawa's stratigraphic equivalent in Kansas, the Tonganoxie Sandstone (Cashman, 2011).

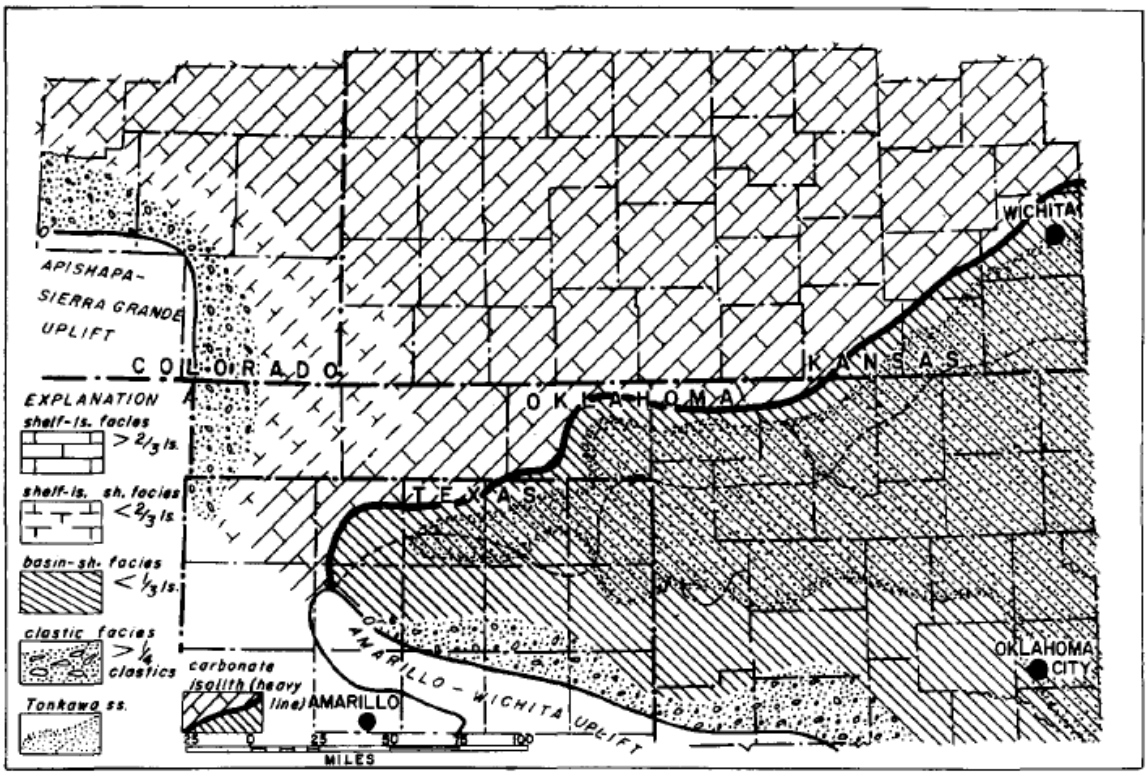

Figure 6: Tonkawa deposition, prograding from the east (Rascoe, 1962).

Chapter 2: Methods

Core Analysis

Three slabbed whole cores were described and interpreted for lithology, sedimentary structures, and vertical facies patterns. These cores include the Sun #1 Lockhart, the Hamon #A-3 Humphreys, and the Internorth #1-46 Humphreys. The Sun #1 Lockhart and the Hamon #A-3 Humphreys wells are located in Feldman oil and gas field in northeastern Hemphill County, Texas. The Internorth #1-46 Humphreys is located in Twister field, approximately three miles southeast of Feldman field (Figure 7). Facies were interpreted by integrating features observed in core with gross-sandstone thickness maps and wireline-log cross sections.

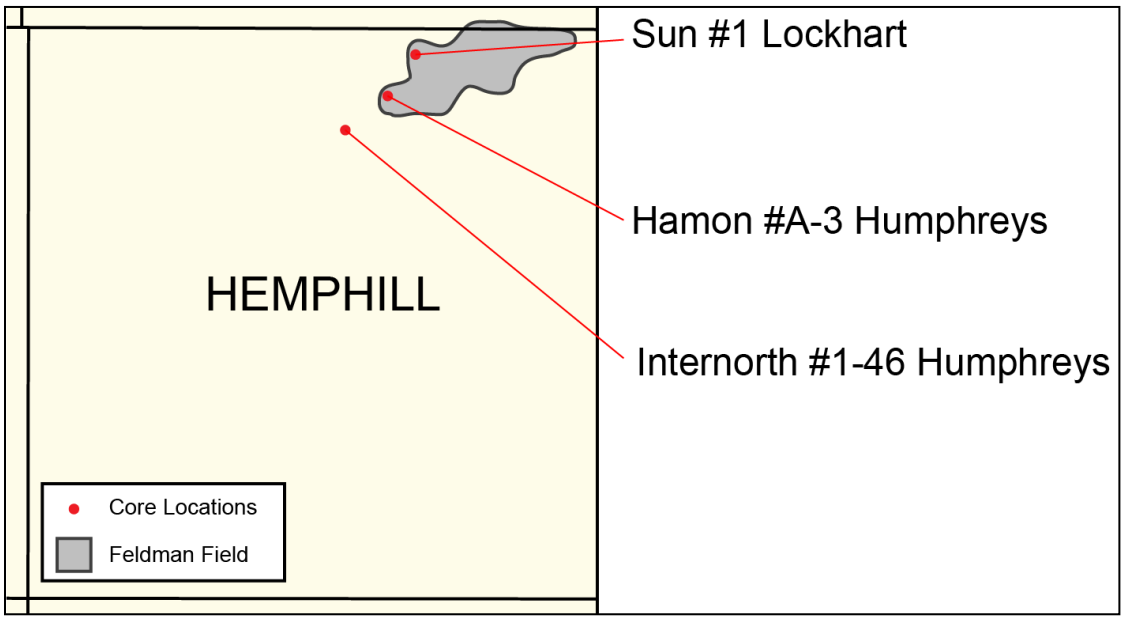

Figure 7: Core locations as well as the location of Feldman oil and gas field in northeast Hemphill County, Texas

Sedimentary structures recorded in core descriptions include wavy, lenticular, and flaser bedding, cross bedding, plane bedding, rhythmic stratification, bidirectional ripple bedforms,

double-draped ripple bedforms, starved ripple bedforms, organic matter, burrows, bioturbation, clay clasts, soft sediment deformation and erosional contacts. Variations in lithology between sand-rich and mud-rich intervals were observed, as well as the presence of detrital coal. Based on changes in lithology, vertical stacking patterns and sedimentary structures, significant stratigraphic surfaces such as sequence boundaries and maximum flooding surfaces were defined. Significant surfaces observed in core were then matched to wireline-log response for the purpose of correlations and subsurface mapping.

Subsurface Mapping

Previously work defined lower, middle, and upper Tonkawa stratigraphic intervals (Kumar and Slatt, 1984), employing a lithostratigraphic method of correlation. In contrast, this study defines Tonkawa units in a chronostratigraphic method based on systems tracts bounded by significant stratigraphic surfaces such as sequence boundaries, transgressive surfaces, and maximum flooding surfaces. Stratigraphic surfaces were placed based on changes in depositional patterns within the interval.

Subsurface mapping of the Tonkawa Sandstone was performed using wireline- log data with the IHS software program Petra. Correlations were made using well logs, primarily the gamma ray log. The gamma ray log detects radioactive elements such as potassium, thorium, and uranium: elements commonly closely associated with clay-rich sediments. Thus, the gamma-ray log was used as a close proxy for clay content. The distribution of clay-rich sediments versus sand-rich sediments is key in understanding depositional patterns, thus the gamma ray log was the primary log curved used for correlations. Correlations in the study area were made by observing changes in depositional patterns according to stacking pattern changes observed in

well log data. Maximum Flooding Surfaces (MFSs) were placed at the top of large, regional fining-upward patterns on the gamma ray log. Transgressive Surfaces (TSs)/ Sequence Boundaries (SBs) were placed at the top of large, regional coarsening-upward patterns observed on the gamma ray log.

Gross sandstone was counted from slabbed core, which was then calibrated to gamma ray log response. The average gross sandstone approximation equated to approximately 15 API to the left of the shale baseline. Gross sandstone maps were constructed for three intervals within the Tonkawa Sandstone: TST-3, HST-3, and HST-2. Each of these intervals is represented in core. Gross sandstone maps were not constructed for TST-2, TST-1, or HST-1 (Figure 9) because of an absence of sand based on our gross sandstone approximation. Preliminary gross sandstone maps were made in Petra but were improved with hand-drawn contours in order to match sandstone body geometries associated with depositional environments and their facies interpreted from core analysis.

Permeability and Porosity Measurements

Permeability data from cores was obtained using a minipermeameter and from core plug analysis. The minipermeameter employed a pressure-decay system to measure permeability values from 0.001 md to >30 darcys. Permeability values were corrected for slip (Klinkenberg) and for non-darcian flow (Forchheimer Factor [Forchheimer, 1901; Huang and Ayoub, 2006]). Core plug analysis, employed the Darcy's Law method by testing core plug samples with air as the fluid at a confining pressure of 400 psi. Permeability values taken using Darcy's Law method were slightly less than values measured from the minipermeameter.

Porosity measurements were made using helium injection, known as Boyle's Gas Law method. Both Darcy's Law permeability measurements and helium injection porosity measurements were made on plugs taken from slabbed core. Permeability versus porosity semilog crossplots such as those employed by Ehrenberg (2006) were constructed using porosity values taken from helium injection tests and permeability measurements obtained using the minipermeameter. Minipermeameter values were more abundant, and therefore were used for crossplots instead of values obtained using Darcy's Law method. Samples were organized on the crossplot according to their respective facies. Facies interpretations were based on interpretations made from core analysis and gross-sandstone thickness maps.

Petrography

Sixteen thin sections were prepared from cuttings taken from core plugs used in permeability and porosity measurements. Thin sections analyzed represent samples from each facies interpreted from core data. Thin sections were described in terms of mineralogy, porosity, cementation, grain sorting, grain rounding, and particle size. Each thin section was counted with 250 points, counting porosity, dominant framework grains, accessory minerals, and cementation type. A 250-point point count was used based on the "Nomograph For Determination of Counting Error" adapted from Van der Plas and Tobi (1965). Despite relatively high amounts of mud present in various samples, all 16 thin sections were plotted on a quartz-feldspar-rock fragment ternary diagram ternary diagram using methods presented by Folk (1980) in order to determine the classification of sand present within each sample. Refer to Table 2 for a complete list of thin section names, associated wells, depths, and facies.

Chapter 3: Sequence Stratigraphy

The interplay of accommodation and sedimentation within a basin results in the deposition of genetic units which are bound by specific stratigraphic surfaces. These genetic units and their associated stratigraphic surfaces compose a sequence stratigraphic framework (Catuneanu et al., 2009). In this study, stratigraphic surfaces were placed based on changes in depositional patterns. Such patterns include coarsening-upward progradational patterns, aggradational patterns, and fining-upward retrogradational patterns (Figure 8), which are driven by fluctuations in base-level. Base-level can be defined as "an abstract surface that represents a surface of equilibrium between erosion and deposition" (Emery, 2002).

Progradational stacking patterns are associated with periods of time in which sedimentation rates outpaced base-level rise at the shoreline, and are called periods of normal regression (Catuneanu et al., 2009). Retrogradational stacking patterns are associated with periods of time in which sedimentation rates failed to outpace base-level rise and are called periods of transgression. Stratigraphic stacking patterns associated with base-level changes can be organized into stratigraphic packages known as systems tracts (Van Wagoner et al., 1990). A systems tract can be defined as a linkage of contemporaneous depositional systems (Brown and Fisher, 1977). Systems tracts are used to subdivide depositional sequences.

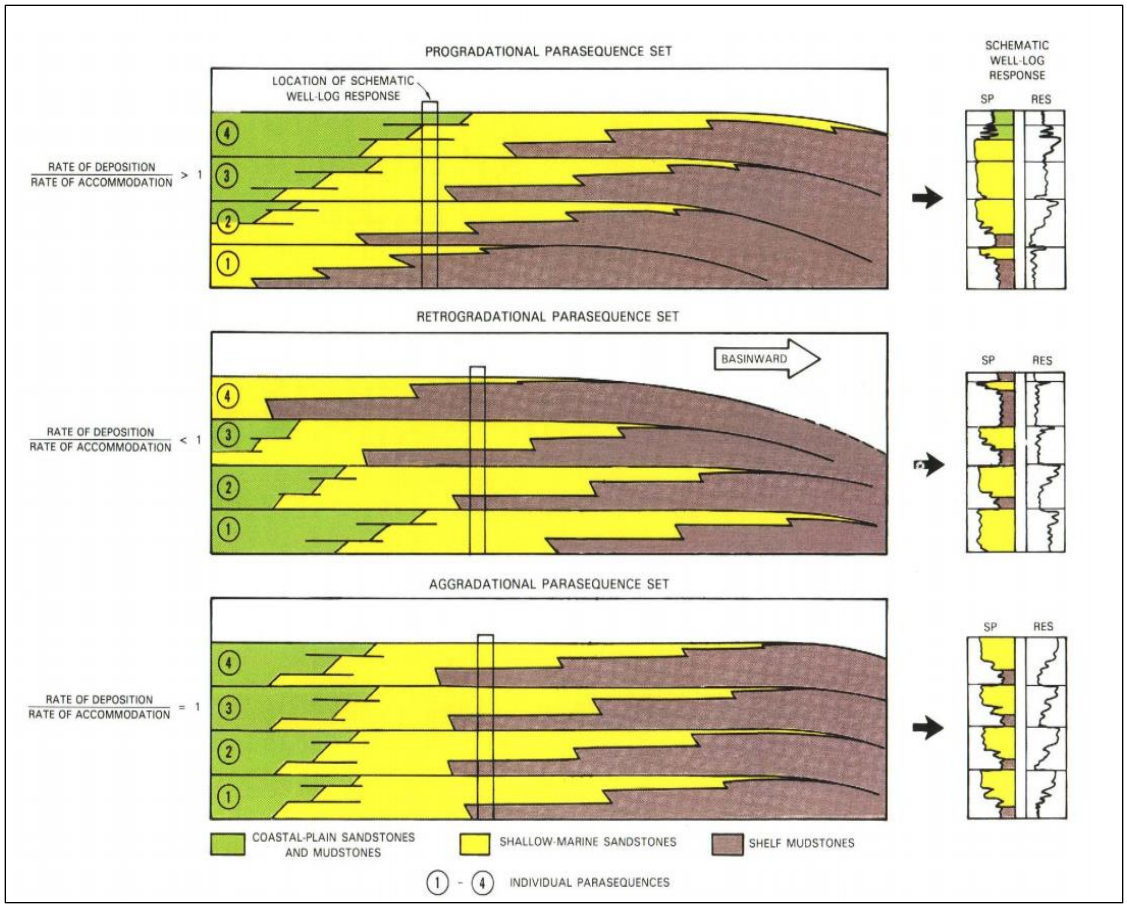

Figure 8: Progradational, retrogradational, and aggradational stacking patterns (Van Wagoner et al., 1988; 1990)

Systems Tracts

Transgressive Systems Tract

The transgressive systems tract, also known as the TST represents a period of rapid eustatic rise and is associated with periods of transgression within a sequence stratigraphic framework. TSTs can thicken landward, reflecting a shift of the depoceneter (Catuneanu et al., 2009). Within our study area, TSTs are characterized by a back-stepping, retrogradational stacking pattern.

Highstand Systems Tract

The highstand systems tract, also known as the HST, is associated with the late part of a eustatic rise, a eustatic stand-still, and eventually an early period of eustatic fall. The HST occurs at the top of a sequence and is associated with periods of regression within a sequence stratigraphic framework. HSTs deposited as a result of sedimentation outpacing base-level rise at the shoreline are called highstand normal regressive (HNR) systems tracts (Catuneanu, 2006). Within our study area, HSTs are characterized by large, regionally-extensive progradational intervals and are interpreted to be highstand normal regressive systems tracts (HNRs). From this point forward, all HSTs described within the study area are considered HNRs. Both TSTs and HSTs are bound by specific stratigraphic surfaces. In this study, two main stratigraphic surfaces were used.

Stratigraphic Surfaces

Transgressive Surface (TS)

The transgressive surface (TS), also known as the maximum regressive surface (MRS), represents the first significant marine-flooding surface across the shelf within a sequence (Van Wagoner et al., 1987). This surface forms during base-level rise and marks the change in depositional pattern from progradation to retrogradation (Catuneanu et al., 2009). The TS forms the base of the transgressive systems tract, and marks the top of a lowstand systems tract lowstand wedge, if fluvial incision occurs across the shelf during sea-level lowstand (Van Wagoner et al., 1988). If incision does not occur, the TS represents a sequence boundary, or SB, as well. Within the study area, no evidence of shelfal incision was found, thus transgressive surfaces (TSs) are also representative of sequence boundaries (SBs). The conformable

relationship between TSs and SBs can been seen in Figure 9. SBs represent the top of HSTs as well as the base of TSTs. From this point forward, the term "SB" will exclusively be used in place of "TS."

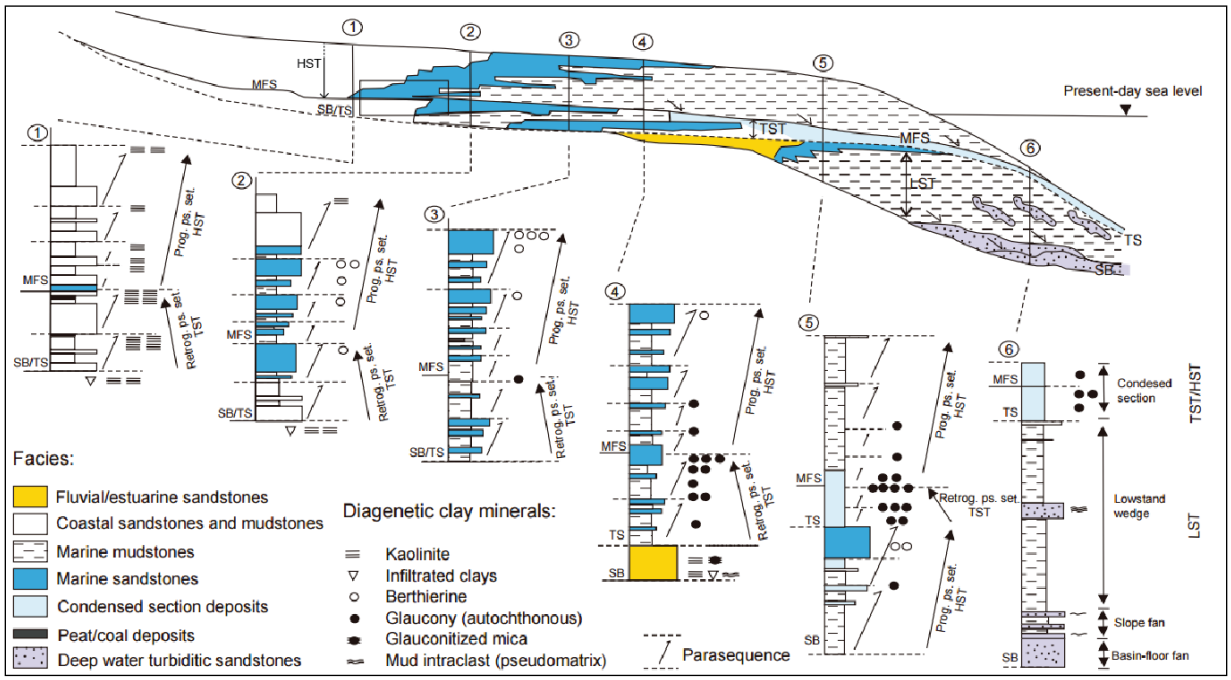

Figure 9: Systems tracts, stratigraphic surfaces, and facies within a sequence stratigraphic framework. In more landward facies diagrams (1-3) SBs and TSs represent the same surface. (Modified from Catuneanu, 2006 and Ketzer, 2003)

In core, SBs are found at the top of large coarsening-upward intervals, marking the point of maximum regression before sediments exhibit a fining-upward pattern. When matched to wireline-log response, SBs are regionally correlative and occur at the top of large coarsening-upward patterns observed in the gamma-ray log.

Maximum Flooding Surface (MFS)

The maximum flooding surface, or MFS, is a marine flooding surface which represents the highest relative sea level and the change from a retrogradational stacking pattern to an aggradational or progradational stacking pattern. Aggradation occurs when sedimentations keeps pace with base-level rise, meanwhile progradation occurs when sedimentation outpaces base-level rise (Van Wagoner et al., 1988). The MFS is a downlap surface, onto which the "toes" of prograding clinoforms, such as those associated with the HST, downlap. MFSs represent the top of TSTs, as well as the base of HSTs.

In core, MFSs are found at the top of large fining-upward intervals, marking the point of maximum transgression. Below MFSs, marine condensed section deposits can be observed in distal settings and marine mudstone and sandstones can be observed in more proximal settings. MFSs, when matched to wireline-log response are regionally correlative and occur at the top of fining-upward patterns observed in the gamma-ray log.

Tonkawa Stratigraphy

Within the study area, the Tonkawa Sandstone is divided into three high-order transgressive-regressive sequences, and one larger lower-order sequence, encompassing the higher-order sequences. Each high-order sequence consists of a TST and a normal regressive HST, and is bound above and below by sequence boundaries. Repetitive successions of transgressive and normal regressive deposits such as these are known to occur in basins such as the Anadarko Basin, where continuous base-level rise outpaces and is outpaced by sedimentation in a cyclic manner (Catuneanu, 2006).

Surfaces mapped within the study area include MFS-0, SB-1, MFS-1, SB-2, MFS-2, SB-3, and MFS-3 (Figure 10)**.** The Haskell and Avant Limestones in Oklahoma are bounding surfaces for the Tonkawa Sandstone. Within our study area, these transgressive limestones grade into distal mudstones. The tops of these mudstones coincide with two regional maximum-flooding surfaces. The lower bounding surface, MFS-0, represents the first maximum flooding surface and occurs at the top of a retrogradational, open-marine shale approximately 250-350 ft. thick throughout the study area. MFS-0 is considered to be genetically equivalent to the Avant Limestone. MFS-0, like the Avant Limestone represents the first change from retrogradation to progradation, beginning Tonkawa deposition. The uppermost bounding surface, MFS-3, is a basin-wide "hot shale" marker placed at the top of a large open-marine shale, and is genetically equivalent to the Haskell Limestone. This was confirmed through lithologic observations made in the Hamon #A-3 Humphreys core and the Sun #1 Lockhart core that were then tied to wireline log response in cross section across the study area.

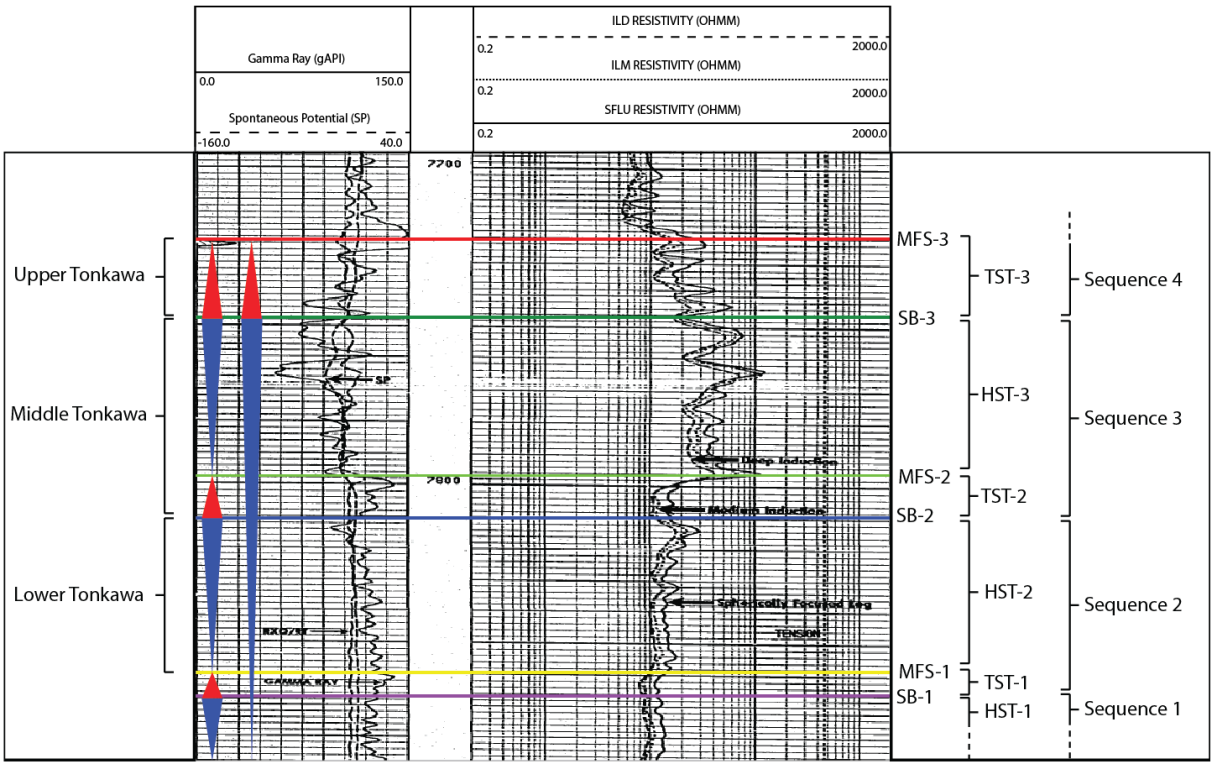

Figure 10: Tonkawa Stratigraphic Surfaces: A type log from the study area is labelled with the stratigraphic surfaces mapped throughout the study area. Stratigraphic surfaces bound respective systems tracts. Accommodation triangles also show the 3 higher-order transgressive-regressive sequences that composes the Tonkawa Sandstone, as well as the larger lower-order sequence. Bounding surfaces and interval names to the right of the type log are chronostratigraphic surfaces and intervals. Interval names left of the type log represent the three-member lithostratigraphic intervals recognized in previous work on the Tonkawa Sandstone (Upper, Middle, and Lower Tonkawa.) While lithostratigraphic and chronostratigraphic correlations are similar in this log, this is not true throughout the study area. Lithostratigraphic correlations for the Tonkawa Sandstone are placed at the three major intervening shales. These shales however are not correlative across the study area, nor are they representative of genetically-related rock units across the study area. Chronostratigraphic surfaces do however represent genetically-related rock units based on common depositional stacking patterns, thus these surfaces are representative of true Tonkawa Sandstone deposition.

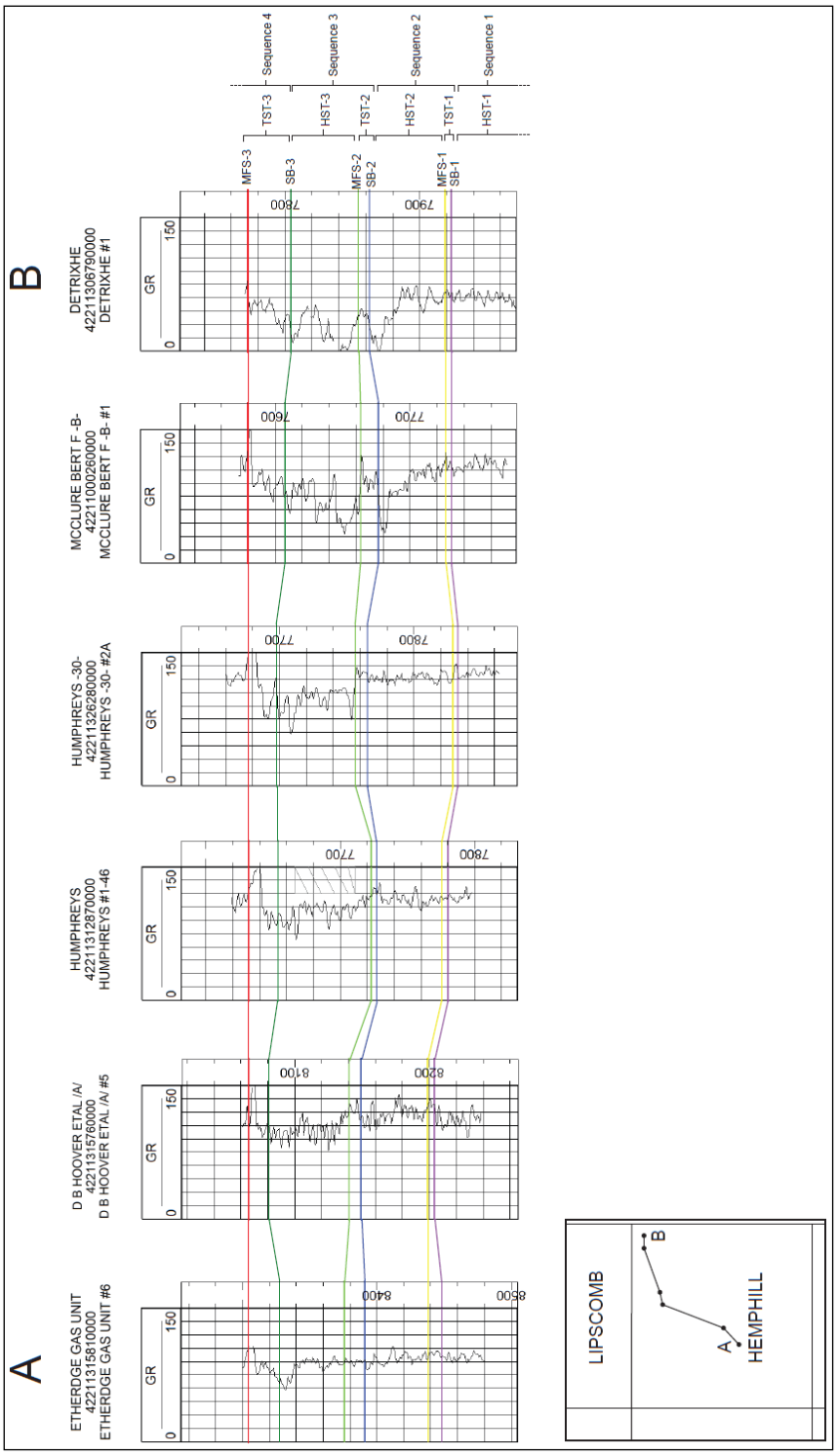

Figure 11: Dip-oriented cross section across the study area from point A to point B (SW-NE). The Internorth #1-46 Humphreys is the third well log from point A.

Chapter 4: Results

Core Descriptions

Sun #1 Lockhart

The Sun #1 Lockhart spans the majority of HST-3 as well as all of TST-3. The cored interval is dominated by very fine-grained sandstone and mudstone beds. At the base of the core, from 7654-7657 ft., a heavily bioturbated mudstone with starved ripples and a clam burrow (Figure 12) coarsens-upward into a siltstone.

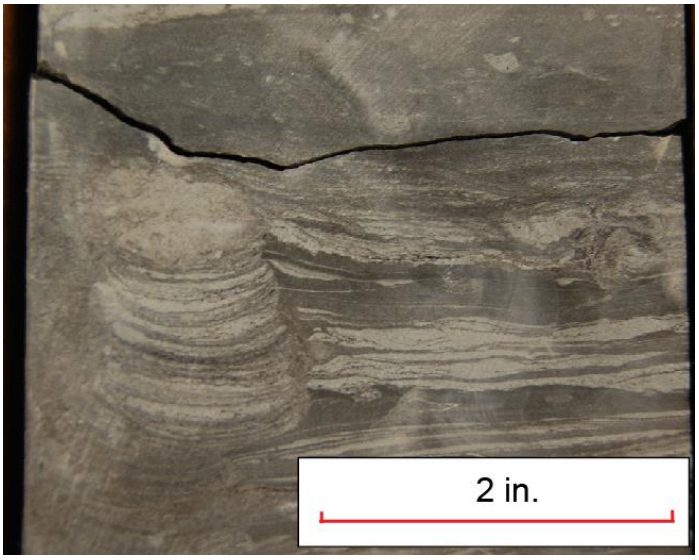

Figure 12: A clam burrow observed at a depth of 7656.5 ft. in the Sun #1 Lockhart

This coarsening upward is the transition from DBS facies to DDTB facies. From 7651-7654 ft. the core is missing, but is then overlain by sandstone with crossbedding, ripple bedforms, plant fragments, and clay clasts which represents the PDTB facies. This interval fines-upward once

again into DDTB facies with alternating siltstones and mudstones with starved ripple bedforms, minor bioturbation, lenticular bedding, and flaser bedding, to a depth of 7636 ft. where an erosional contact is observed. Above the erosional contact, a coarsening-upward PDTB facies is present until a depth of 7621 ft.; Observed features include wavy bedding, ripple bedforms, double-draped ripple bedforms, crossbedding, and an overall increase in sandstone. Above the PDTB facies observed from 7621-7636 ft., the interval begins to fine-upward in a TETB facies that is highly heterolithic. Sedimentary structures include ripple bedforms, upper-flow regime planar stratification, climbing ripples, crossbedding, clay clasts, flaser bedding and soft sediment deformation in mudstone beds. Detrital coal occurs at approximately 7604 ft., as well as plant fragments that appear to be wood and tree bark (Figure 13). At the top of this TETB interval, bidirectional ripples occur (Figure 14).

Figure 13: Tree bark and detrital coal observed within the TETB facies at a depth of 7604 ft. in the Sun #1 Lockhart

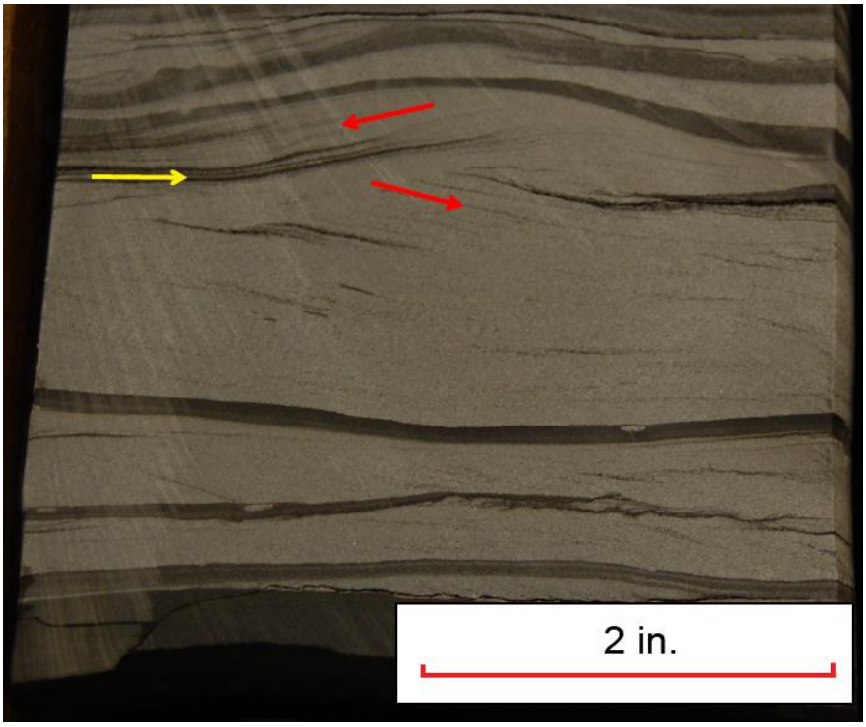

Figure 14: Bidirectional ripple bedforms and double-mud drapes observed within the TETB facies at a depth of 7589 ft. in the Sun #1 Lockhart. Red arrows show ripple foresets deposited in opposite directions and the yellow arrow shows a double-mud drape.

The fining-upward pattern observed in the TETB facies continues into the DS facies which occurs from 7579-7585 ft. This interval is rich in mudstone with starved ripple bedforms, soft sediment deformation, and clay clasts. Above this DS facies interval, the core begins to coarsen-upward with a DDTB facies observed from7574-7579 ft. This DDTB facies interval in more sand-rich than the underlying DS facies interval and has ripple bedforms and clay clasts. As sediments in the core continue to coarsen-upward, a PDTB facies is observed displaying ripple bedforms, clay clasts, upper-flow regime planar stratification, and cross-bedding (Figure 14).

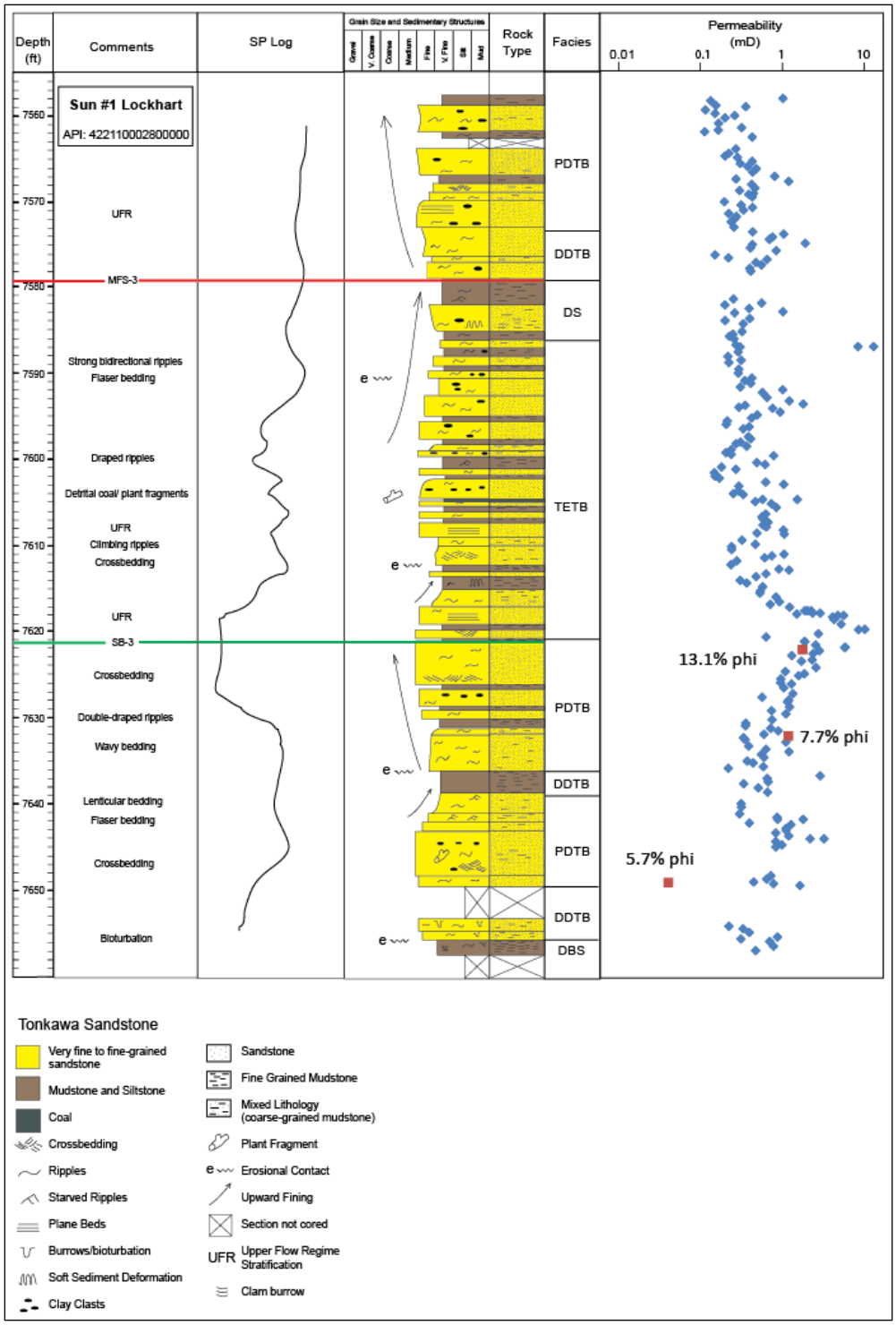

Figure 15: Core description of the Sun #1 Lockhart, Hemphill County, Texas (Figure 7).

Internorth #1-46 Humphreys

The Internorth #1-46 Humphreys spans 45 ft. of HST-3. The core is dominated by very fine-grained sandstone and mudstone beds, with relatively greater mudstone content than that observed in the Sun #1 Lockhart core. The lowermost interval from 7708-7711 ft. is a fissile mudstone with thin interbedded sandstone layers, with starved ripple bedforms, representing the DS facies. This interval is separated from the overlying interval by a sharp erosional contact. The overlying interval spans from 7683-7708 ft. and represents the DDTB facies. Within this interval, flaser bedding, ripple bedforms, starved ripple bedforms, soft sediment deformation, bioturbation and a clam burrow were observed (Figure 16).

Figure 16: A clam burrow observed within the DDTB facies at a depth of 7688.5 ft. in the Internorth #1-46 Humphreys

This DDTB facies interval fines-up to a DS facies interval that spans from7677-7683 ft. Similar to the lowermost DS interval observed in the core, this interval is a fissile mudstone with thin interbedded layers of sandstone and starved ripple bedforms. The core coarsens-up from the top

of this DS facies interval back to a DDTB facies interval which spans from 7666-7677 ft. Within this DDTB facies interval clay clasts, ripple bedforms, and flaser bedding was observed (Figure 17).

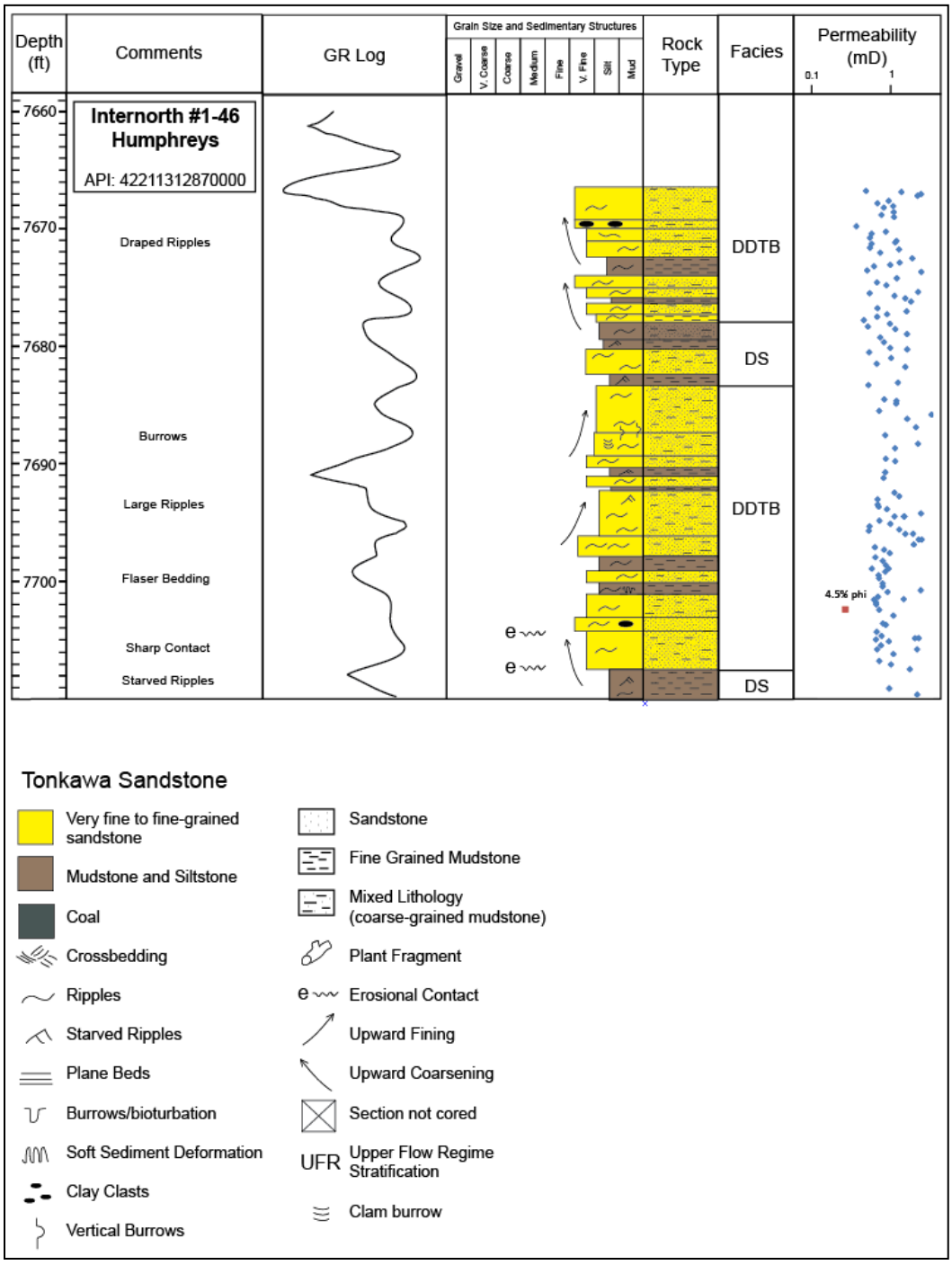

Figure 17: Core description of the Internorth #1-46 Humphreys, Hemphill County, Texas (Figure 7).

Hamon #A-3 Humphreys

The Hamon #A-3 Humphreys core spans 87 ft. and the entirety HST-3 and TST-3. Very fine-grained sandstone beds, interbedded with and mudstone beds characterize the core. The lowermost interval in the core from 7762-7768 ft. represents the DS facies which is dark, mudstone-rich, fissile, and contains soft-sediment deformation, clay clasts, and starved ripples. Immediately above the DS facies interval is a DBS interval that spans from 7755-7762 ft., which is less fissile than the underlying DS facies interval and is bioturbated. Both the DS facies and DBS facies intervals are within the TST-2 stratigraphic interval. An erosional surface at 7755 ft. represents MFS-2 and the beginning of the HST-3 interval, which is much more sandstone-rich than the underlying TST-2 interval. An interval of DDTB facies spans 7740-7755 ft. and is characterized by mud-draped ripples, burrows, as well as wavy and lenticular bedding (Figure 18).

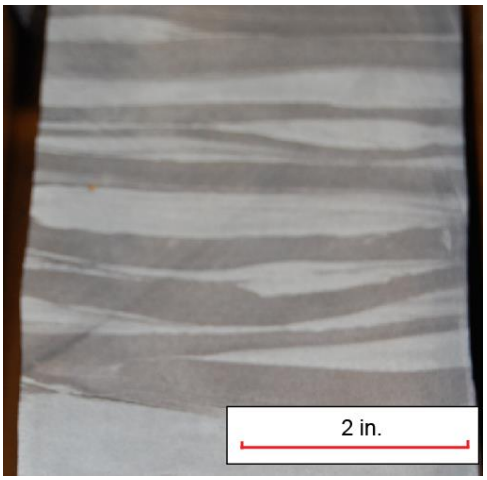

Figure 18: Wavy bedding observed within the PDTB facies at a depth of 7725 ft. in the Hamon #A-3 Humphreys

Overlying this interval is a large upward-coarsening interval of PDTB facies which spans from 7715-7740 ft. Within this interval, ripple bedforms are common, as well as thin clay drapes that increase in width from 0.5-1 cm up-section. Additionally, at the top of this PDTB facies crossbedding is present. Sediments in the core begin to fine upward in a TETB facies interval from 7686-7715 ft. This TETB facies begins as a sandstone-rich interval with sedimentary structures such as clast clasts, ripple bedforms, wavy bedding, crossbedding and soft sediment deformation. The sandstones in this interval are interbedded with mudstones which have starved-ripple bedforms. Above this TETB facies interval is a DBS facies interval from 7682-7686 ft. This DBS facies interval is a dark, bioturbated mudstone with starved ripple bedforms. The top of this interval represents the MFS-3 stratigraphic surface (Figure 19).

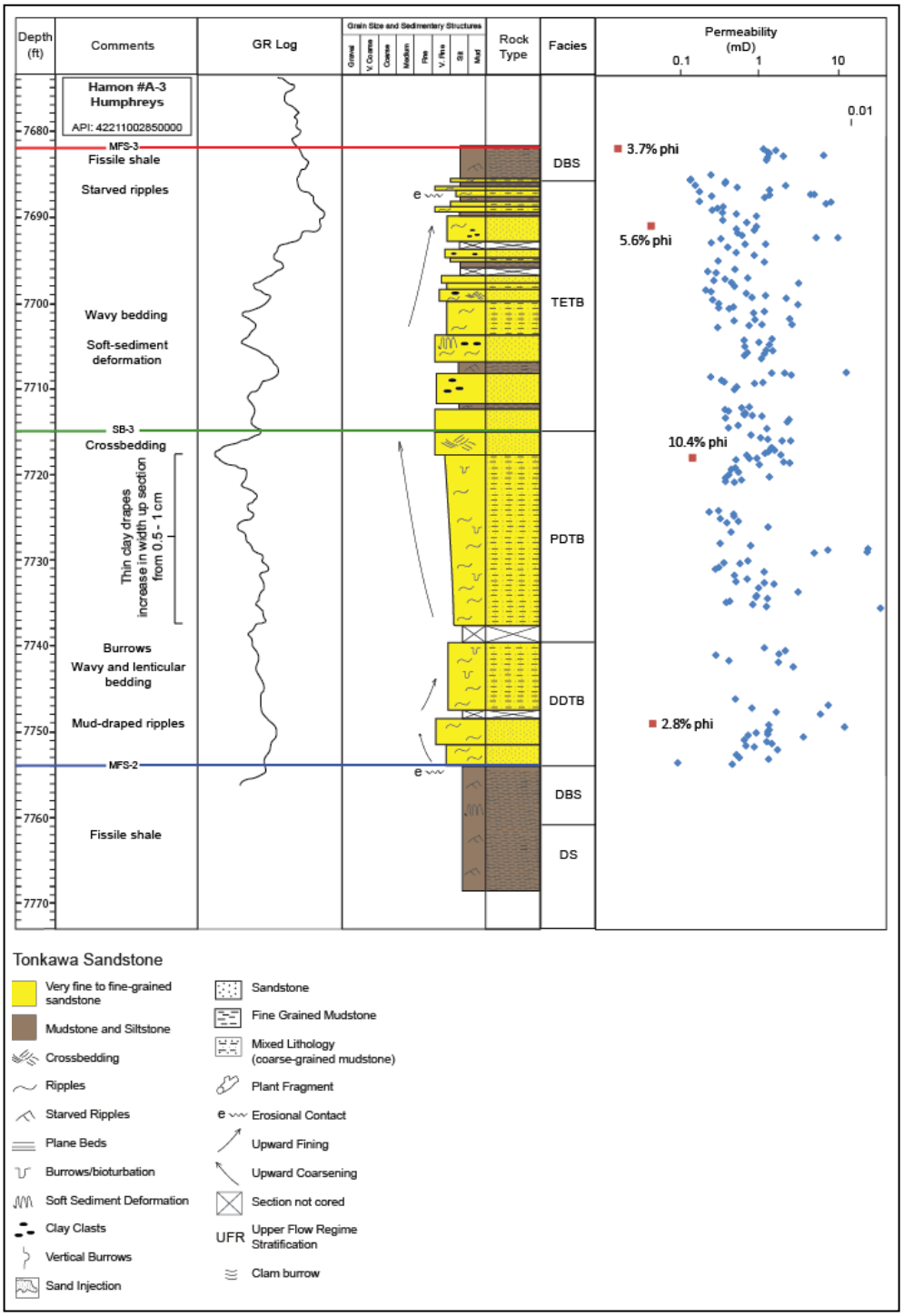

Figure 19: Core description of the Hamon #A-3 Humphreys, Hemphill County, Texas (Figure 7).

Facies Interpretations

Five facies were interpreted in these cores: (1) Distal Bioturbated Shelf (DBS); (2) Distal Deltaic Tidal Bar (DDTB); (3) Distal Shelf (DS); (4) Proximal Deltaic Bar (PDTB); (5) Transgressive Estuarine Tidal Bar (TETB).

Distal Bioturbated Shelf (DBS)

The DBS facies is predominantly mud-rich with sparse starved ripples and contains abundant burrows (Figure 20). Bioturbation can commonly amalgamate sediments and obstruct recognizable sedimentary structures.

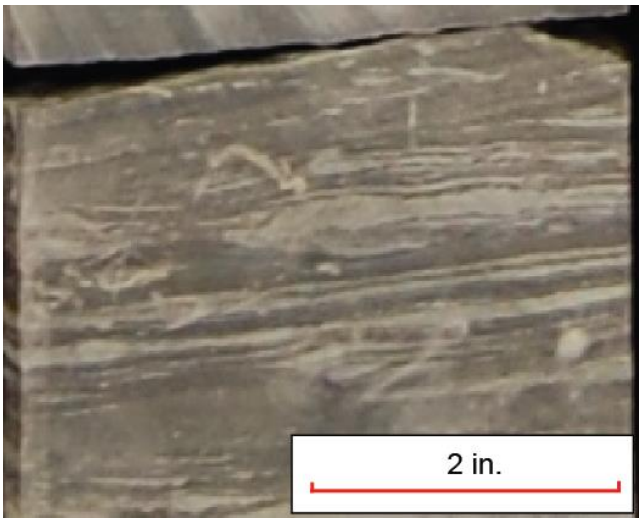

Figure 20: An example of DBS facies at a depth of 7656 ft. in the Sun #1 Lockhart core.

Distal Shelf (DS)

The DS facies is the most mudstone-rich facies observed in core. It is similar to the DBS facies. However, burrows and bioturbation are absent. This facies is also commonly fissile (Figure 21).

Figure 21: An example of DS facies at a depth of 7766 ft. in the Hamon #A-3 Humphreys core.

Distal Deltaic Tidal Bar (DDTB)

The DDTB facies is heterolithic, with varying proportions of sandstone and finer-grained sediments (Figure 22). This facies is dominated by double mud-draped ripple bedforms, as well as bidirectional ripple bedforms, wavy, flaser, and lenticular bedding. Bioturbation also occurs within this facies. This facies occurs at the base of large, upward-coarsening intervals.

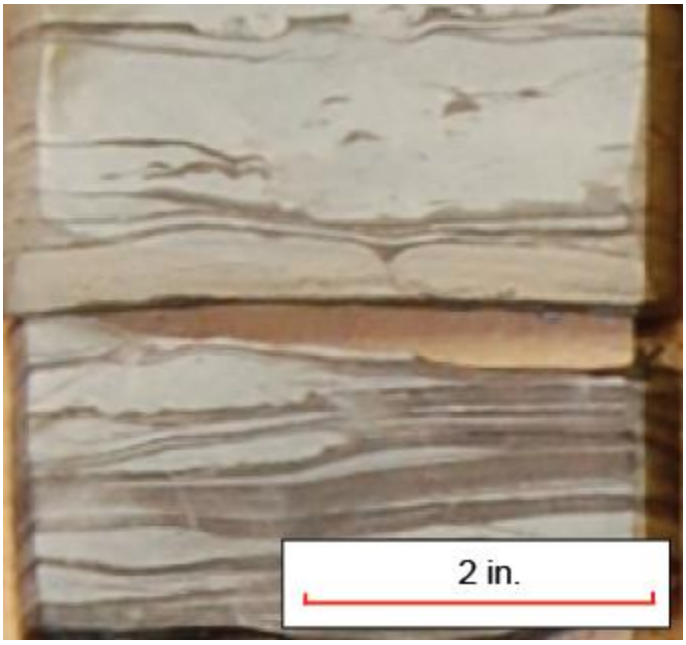

Figure 22: An example of DDTB facies at a depth of 7741.5 ft. in the Hamon #A-3 Humphreys core.

Proximal Deltaic Tidal Bar (PDTB)

The PDTB facies is characterized by clean sandstones with minor mud drapes, crossbedding, and ripple bedforms and thin mud flasers. Bioturbation is completely absent within this facies (Figure 23). This facies occurs toward the top of large, upward-coarsening intervals, above DDTB facies.

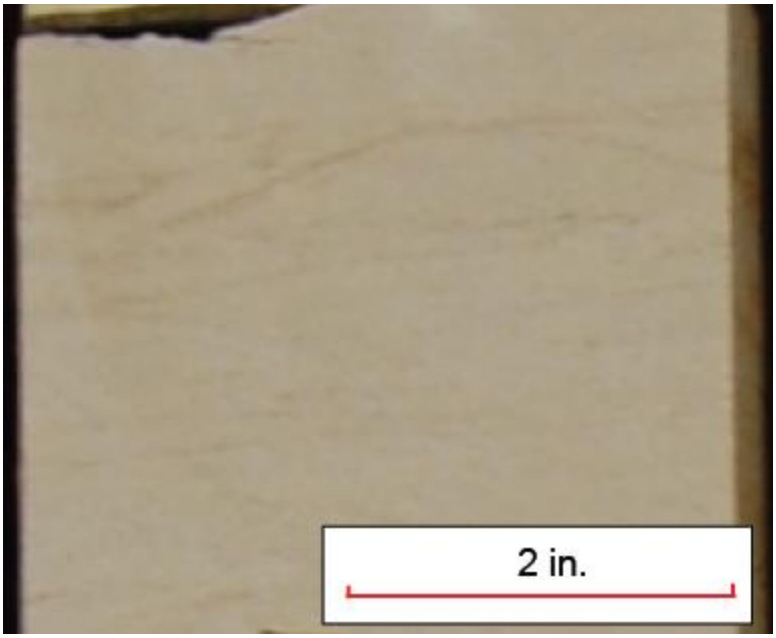

Figure 23: An example of PDTB facies at a depth of 7621.75 ft. in the Sun #1 Lockhart core.

Transgressive Estuarine Tidal Bar (TETB)

The TETB facies is similar to the PDTB facies in terms of sedimentary structures. This facies is highly heterolithic. Clean sandstones are commonly observed at the base of TETB facies intervals with an increase in interbedded mudstones up-section. Plant fragments and detrital coal occur in this facies in the Sun #1 Lockhart core. Additionally, bioturbation is absent (Figure 24). This facies occurs at the base of larger retrogradational intervals, above PDTB facies.

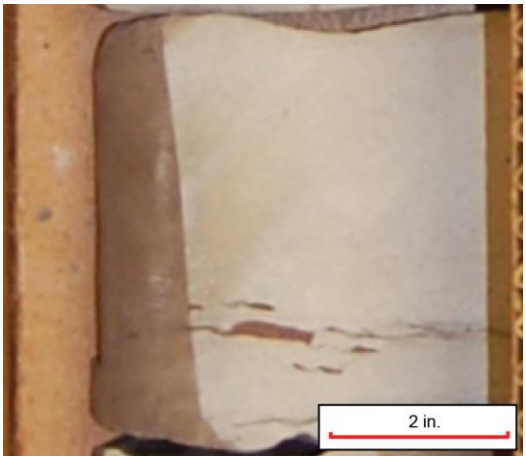

Figure 24: An example of TETB facies at a depth of 7711 ft. in the Hamon #A-3 Humphreys core.

Sandstone-Body Distribution

HST-2 (Figure 10), which represents the highstand systems tract within the second sequence observed during Tonkawa deposition, is the lowermost sand-rich interval within the study area. Gross sandstone thickness in this interval is as much as 40 ft. across the northeast part of the study area. Moderately sinuous, dip-elongate sandstone bodies with a northeast-southwest orientation extend over ten miles, extending toward other sandstone bodies that are linear and strike-elongate in a northwest-southeast orientation, occurring for tens of miles (Figure 25).

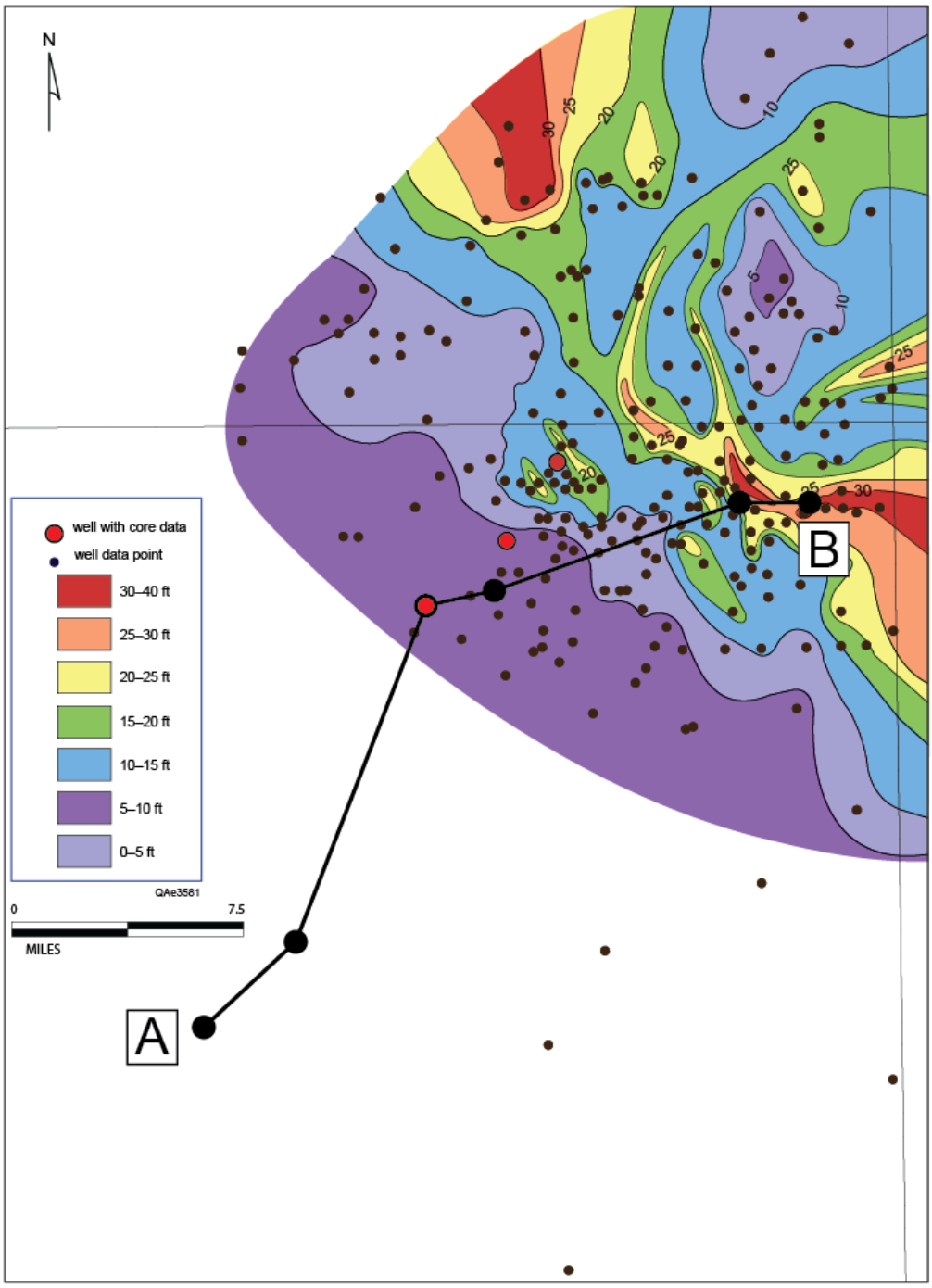

Figure 25: Gross sandstone map of HST-2. Map area is the same as study area, shown in Figure 2. Transect line A-B corresponds to the dip-oriented cross section (Figure 11).

HST-3 represents the highstand systems tract within the third sequence observed during Tonkawa deposition (Figure 10). This interval is much more sandstone-rich than the HST-2 interval. Gross-sandstone thickness in this interval ranges from 0-70 ft. across most of the study area, predominantly within the northeast. In contrast to HST-2, sandstone body geometries within this interval are dip-elongate and dip-parallel, oriented in a northeast-southwest direction. Sandstone bodies in HST-3 are highly elongate, 3-5 mi. in length, and 0.5 mi. in width. The principal orientation of all sandstone bodies in HST-3 is northeast-southwest (Figure 26).

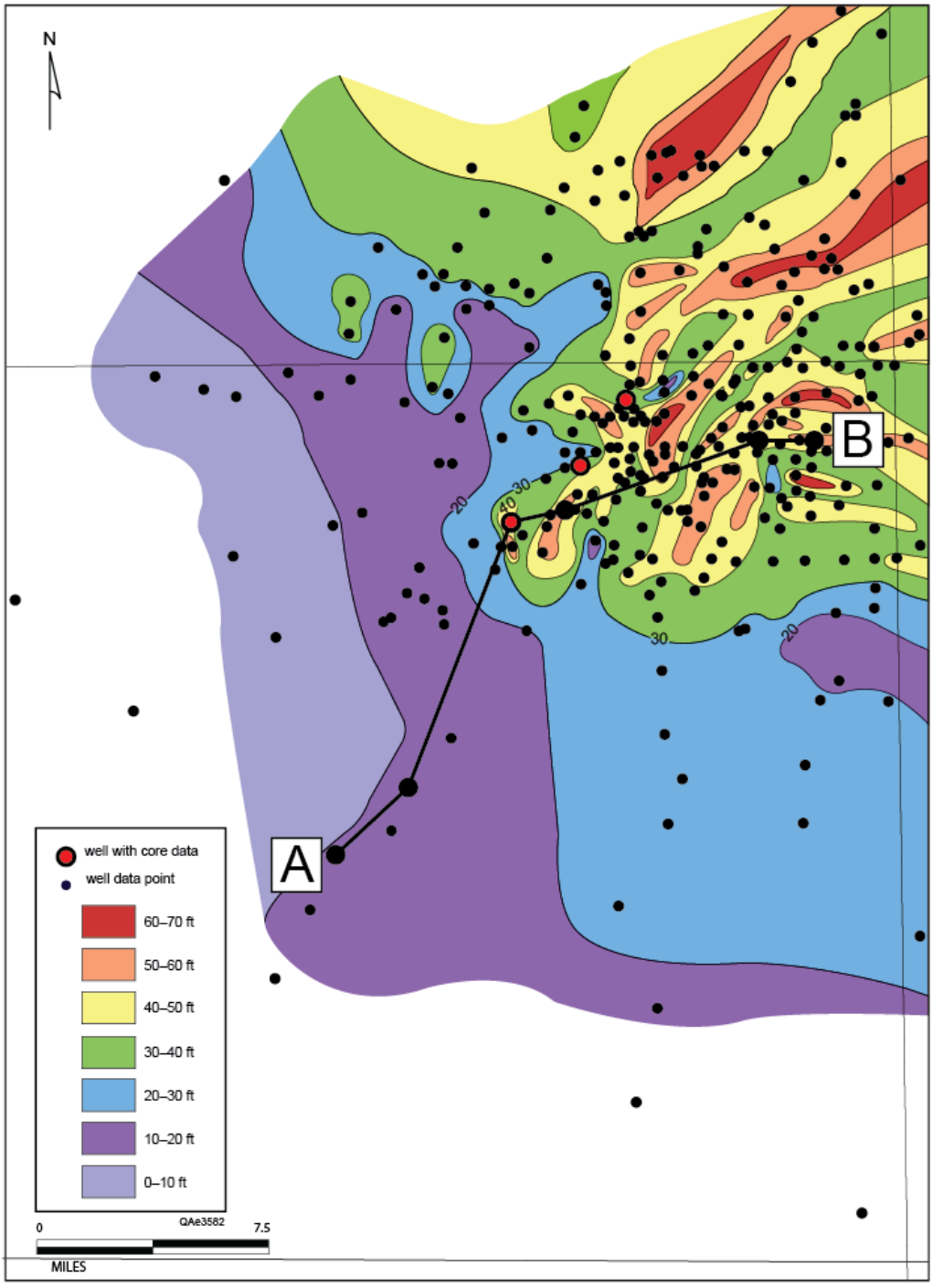

Figure 26: Gross sandstone map of HST-3. Map area is the same as study area, shown in Figure 2. Transect line A-B corresponds to the dip-oriented cross section (Figure 11).

TST-3, which represents the transgressive systems tract of Sequence 3(Figure 10), contains the final sandstone-rich interval deposited within the study area. Although this interval is predominantly mudstone-rich, a well-developed sandstone-rich unit occurs at the base. Sandstone body geometries within this interval display varying orientations are more erratic. In the northeast part of the study area, sandstone bodies display an east-west elongate geometry. Further west within the study area, they are oriented in an elongate northwest-southeast orientation, similar to those in HST-2. Down dip from these elongate sandstone bodies, gross sandstone values significantly decrease (Figure 27).

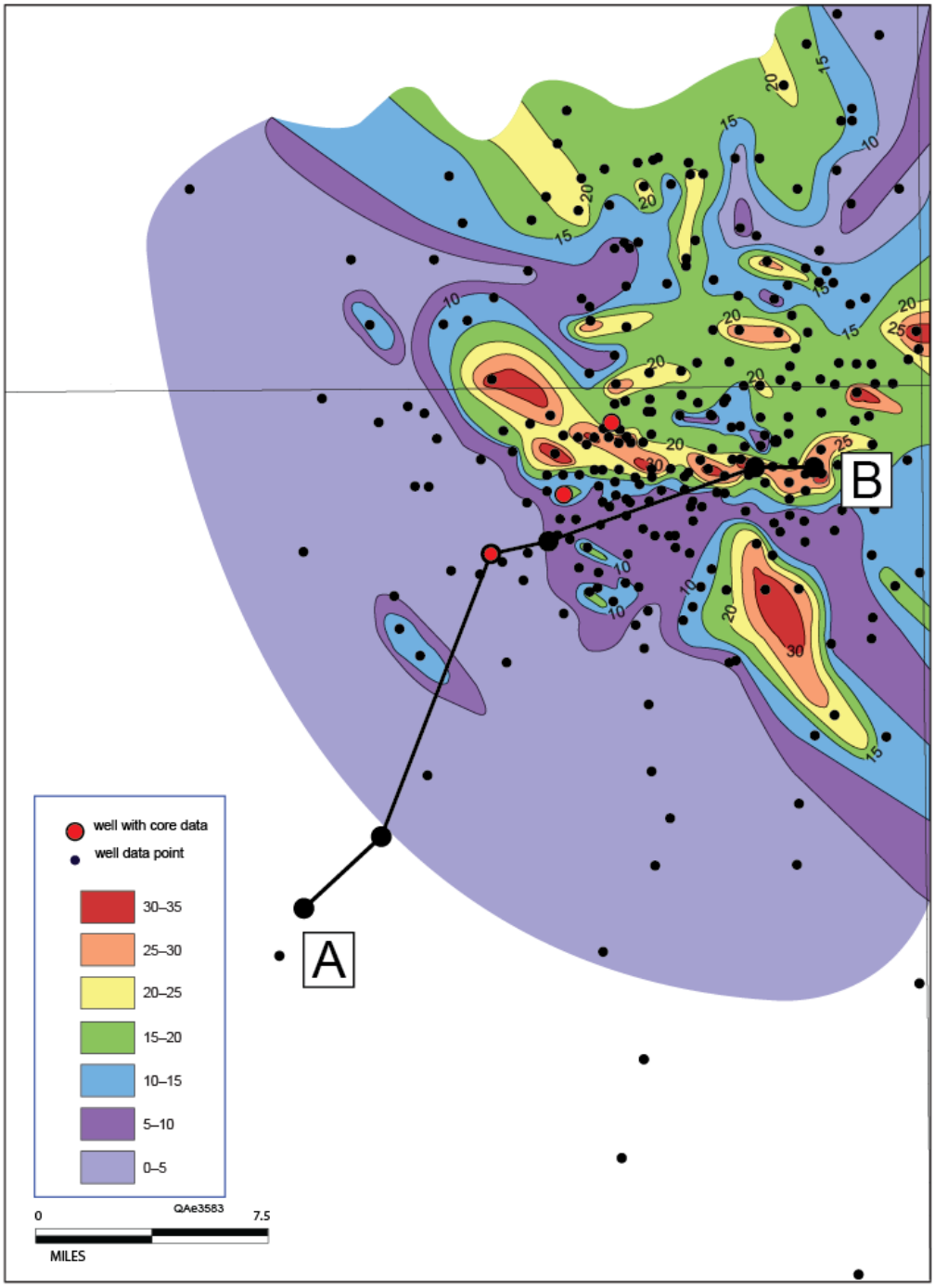

Figure 27: Gross sandstone map of TST-3. Map area is the same as study area, shown in Figure 2. Transect line A-B corresponds to the dip-oriented cross section (Figure 11).

Porosity and Permeability

When plotted a logarithmic vs. linear crossplot of permeability vs. porosity, facies variations are observed (Figure 28). Among all facies, the PDTB facies displays the greatest permeability and porosity values. DDTB facies displays a significant decrease in both permeability and porosity, whereas DS facies displays the lowest permeability and porosity values. DBS facies contain similar porosity values as the DS facies, but with greater permeability. This increase in permeability may be a result of widespread bioturbation reworking sand and mud sediments into an amalgamated lithology, void of sedimentary structures such as mud-drapes and wavy bedding which may act as barriers to flow. TETB facies displays values similar to PDTB facies (Figure 28).

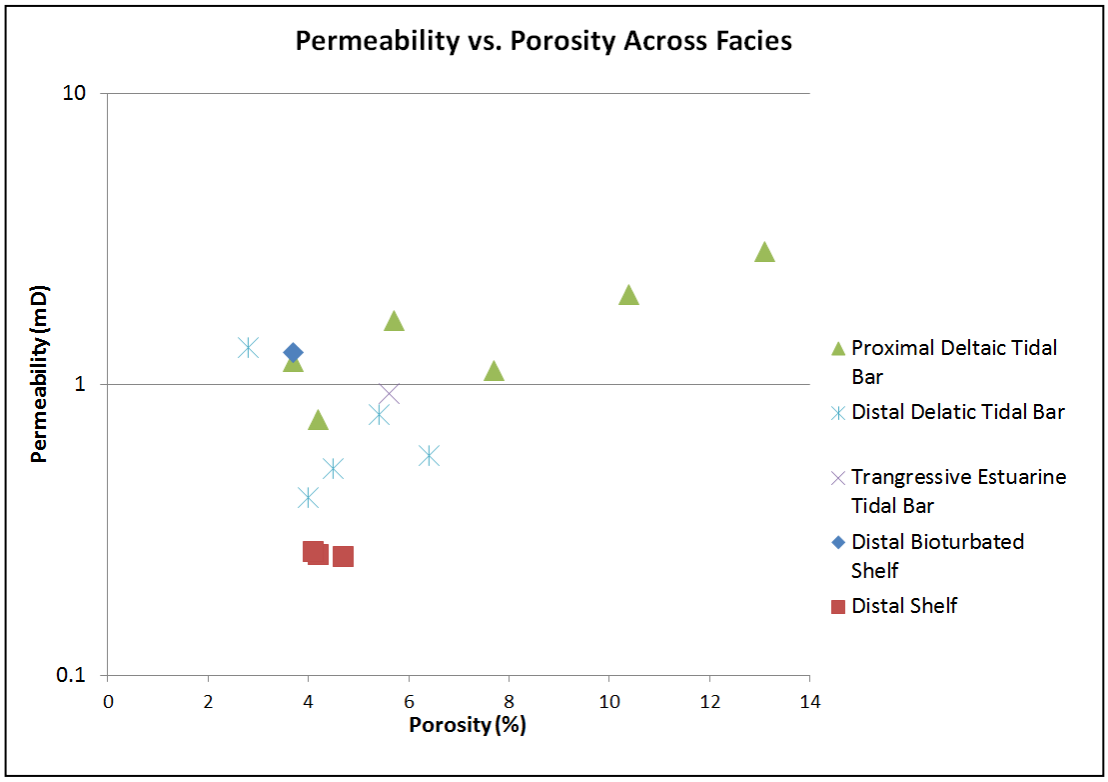

Figure 28: Permeability vs. Porosity crossplot of Tonkawa Sandstone facies.

Average porosity values in facies are: DBS: 3.7%; DDTB: 4.6%; DS: 4.3%; PDTB: 7.5%; TETB: 5.6% (Table 1).

Facies	Sample #	Porosity (%)	Average Porosity (%)
Distal Bioturbated Shelf	H-7682	3.7	3.7
Distal Delatic Tidal Bar	H-7728	5.4	4.6
	I-7698	4.0	
	I-7702.5	4.5	
	H-7749	2.8	
	I-7705.5	6.4	
Distal Shelf	L-7580	4.7	4.3
	I-7678	4.2	
	I-7678.5	4.1	
Proximal Delatic Tidal Bar	H-7718	10.4	7.5
	L-7622	13.1	
	L-7632	7.7	
	L-7649	5.7	
	I-7670	4.2	
	I-7675	3.7	
Transgressive Estuarine Tidal Bar	H-7691	5.6	5.6

Table 1: Porosity values and average porosity values among Tonkawa Sandstone facies.

Within the Tonkawa Sandstone a gradual increase in permeability values occurs within strongly progradational, upward-coarsening-upward intervals such as the HST-3 interval within the Sun #1 Lockhart core (Figures 14 & 25). These upward-coarsening intervals are commonly composed of DDTB facies towards the base, overlain by PDTB facies. Because DDTB facies displays lower permeability values than the overlying PDTB facies, an increase in permeability is often observed as one moves up-section in a coarsening-upward interval. Conversely, there is an associated decrease in permeability as one moves up-section within retrogradational, upward-fining intervals such as the TST-3 interval. Retrogradational intervals such as these are

commonly composed of TETB facies overlain by DS or DBS facies. This permeability trend is best observed in the Sun #1 Lockhart (Figures 15 & 29).

Permeability measurements taken from both the minipermeameter and plug analysis have been plotted together for comparison and labelled accordingly. Permeability measurements obtained using plug analysis have been plotted with measured porosity values as well (Figure 29).

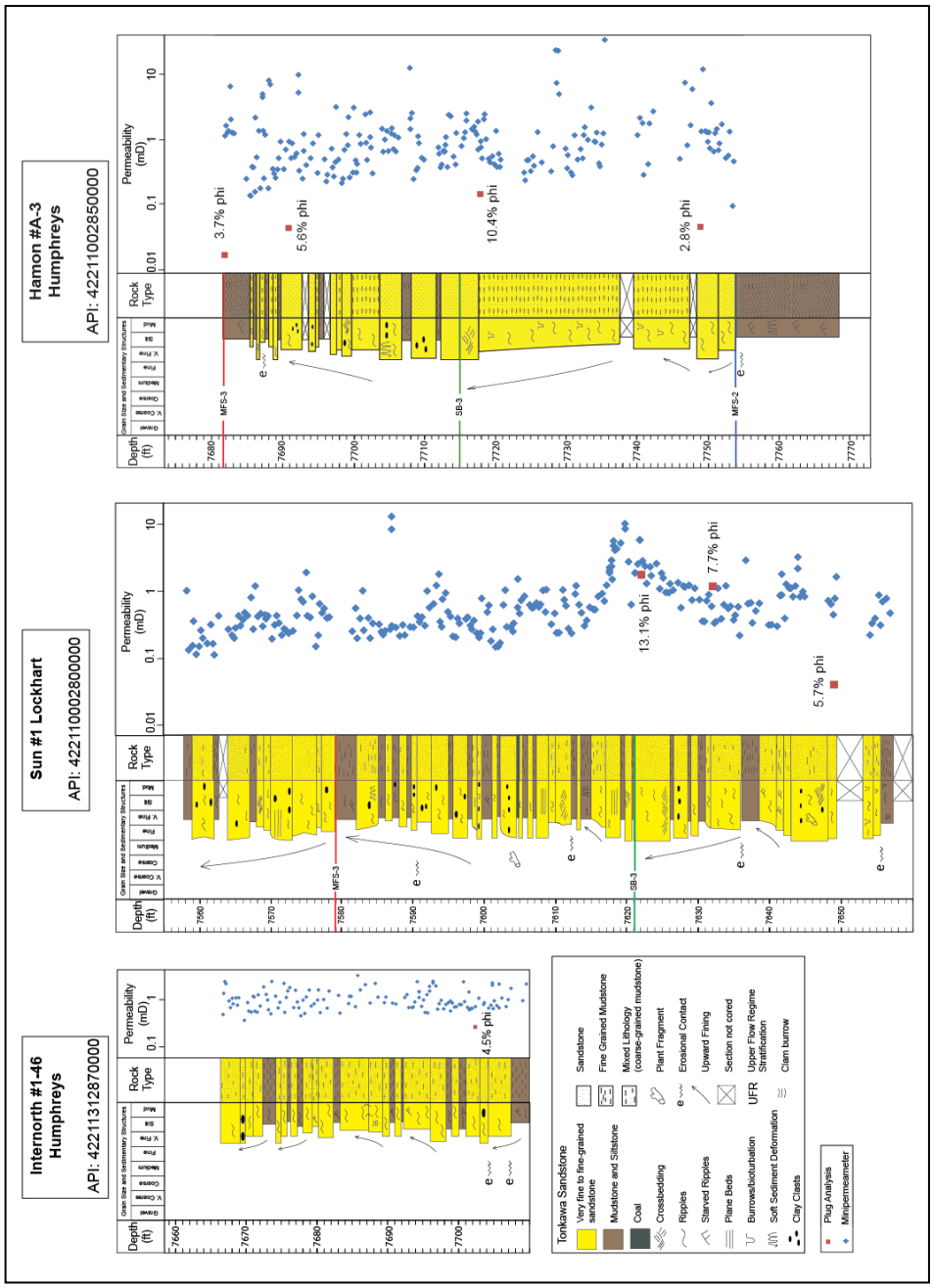

Figure 29: Core Descriptions with Depth vs. Permeability Plot: Data points in blue were obtained using the minipermeameter. Data points in red were obtained using plug analysis (Darcy's Law method) and have been plotted with their associated porosity measurements. Permeability values generally increase in coarsening-upward intervals and decrease in fining-upward intervals. This is best observed in the Sun #1 Lockhart core.

Petrography

Tonkawa sandstones are classified as a sublitharenite to litharenite based on the classification utilized by Folk (1980) (Figure 30). Based on point count data, the average mineral composition for Tonkawa Sandstone samples is $Q_{73}F_0R_{27.}$ Principal framework grains include quartz and metamorphic rock fragments. Common accessory minerals include muscovite, biotite, plagioclase and orthoclase feldspars, chlorite, glauconite, and heavy detrital minerals such as zircons and pyrite. Organic matter commonly occurs in mud-rich samples. Tonkawa sand grains are generally subangular to subrounded and are moderately well-sorted. Depending on the facies each sample has largely different proportions of mud and sand. Samples from more proximal facies such as PDB facies contained no mud while samples from more distal facies such as DS had up to approximately 35% mud.

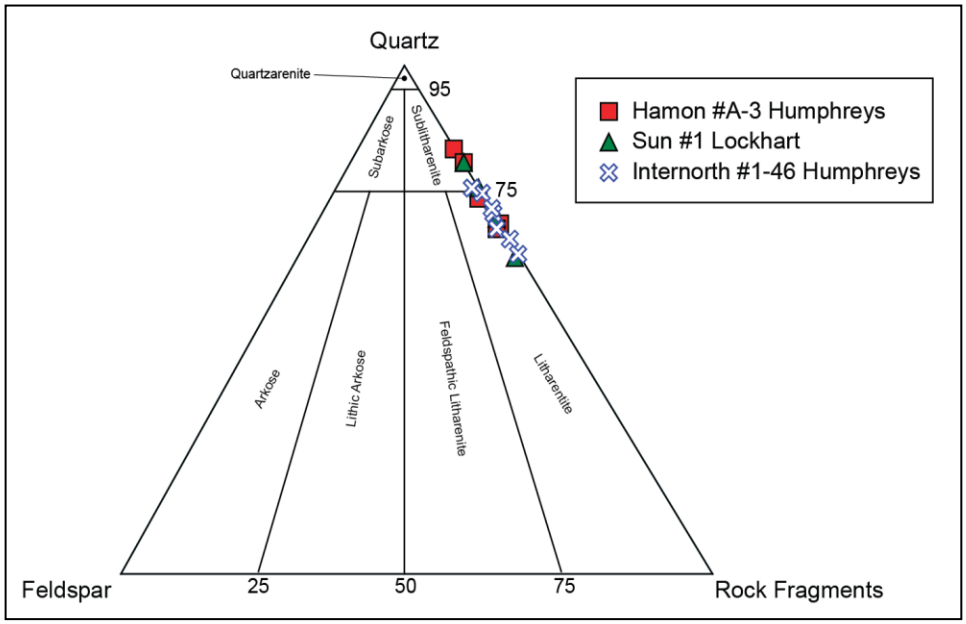

Figure 30: QFR ternary diagram representing a total of 16 Tonkawa thin sections.

			PLUG ANALYSIS		MINIPERMEAMETER	
WELL	SAMPLE	DEPTH	POROSITY (%)	PERMEABILITY (mD)	(mD)	FACIES
HAMON #A-3 HUMPHREYS	H-7682	7682	3.7	0.017	1.29	DBS
	H-7691	7691	5.6	0.044	0.93	TETB
	H-7718	7718	10.4	0.146	2.04	PDTB
	H-7728	7728	5.4	0.003	0.786	DDTB
	H-7749	7749	2.8	0.046	1.34	DDTB
INTERNORTH #1-46 HUMPHREYS	I-7670	7670	4.2	0.477	0.758	PDTB
	I-7675	7675	3.7	TBFA	1.2	PDTB
	I-7678	7678	4.2	0.26	0.26	DS
	I-7678.5	7678.5	4.1	TBFA	0.266	DS
	I-7698	7698	4	TBFA	0.41	DDTB
	I-7702.5	7702.5	4.5	0.071	0.513	DDTB
	I-7705.5	7705.5	6.4	TBFA	0.57	DDTB
SUN #1 LOCKHART	L-7580	7580	4.7	0.256	0.256	DS
	L-7622	7622	13.1	1.788	2.87	PDTB
	L-7632	7632	7.7	1.193	1.12	PDTB
	L-7649	7649	5.7	0.041	1.66	PDTB

Table 2: Thin sections and their associated well, depths, permeability and porosity values, and associated facies. TBFA denotes "too broken for analysis."

Samples H-7682, I-7678, AND I-7678.5 each exhibit a mud-rich matrix, and represent a dominantly mud-rich facies. Samples H-7728, L-7580, L-7632, I-7698, I-7702.5, and I-7705.5 exhibit mudstone occurring in thin mud-drapes, with minor amounts of mud occurring within the matrix. Point count porosity values for Tonkawa sediments vary from 0.4-13.57%. Point count porosity values are commonly less than porosity values obtained using helium injection, particularly in mud-rich samples. This can be attributed to: (1) the inability of point counting to account for the three-dimensional porosity measured in a plug sample; (2) microporosity below the resolution of a petrographic microscope. Tonkawa sandstones typically display primary porosity as well as minor secondary porosity. Primary porosity is commonly occluded by widespread quartz overgrowth (Figure 31). Additionally, ankerite cement and calcite cement are present in thin section (Figures 32 and 33); however these cements are not as common as quartz. Secondary porosity occurs in the form of partially or completely dissolved plagioclase and

orthoclase feldspar grains, and also occurs within fossils such Reophax, a marine organism (Figure 34).

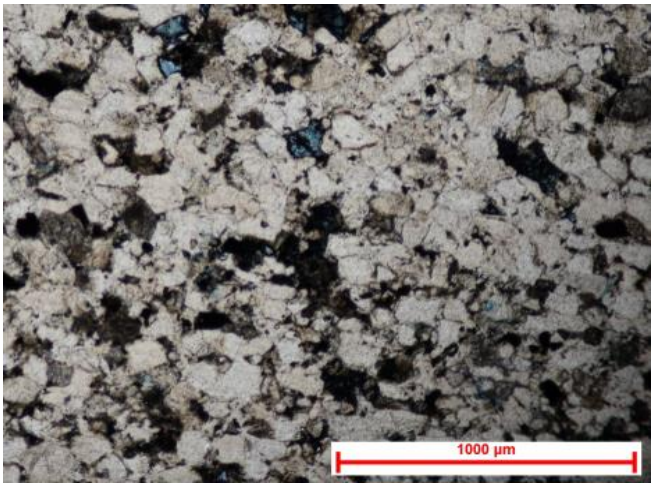

Figure 31: Quartz overgrowth occluding primary porosity in sample H-7691 taken from the Hamon #A-3 Humphreys core at a depth of 7691 ft. within TETB facies. Sample is under 5X magnification in plane polarized light. (H-7691 5X PPL)

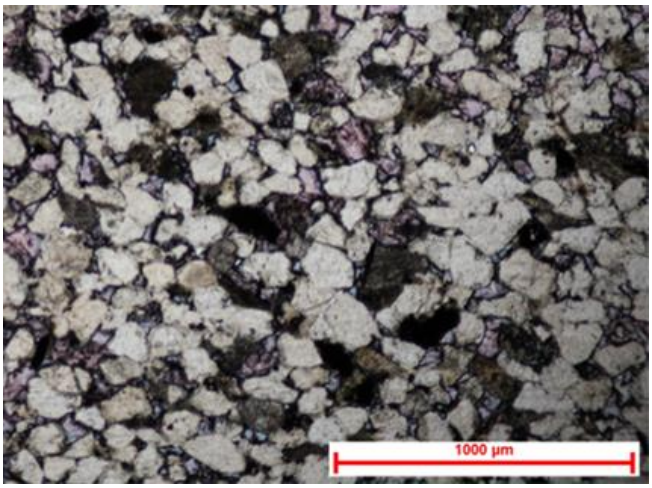

Figure 32: Ankerite cement occluding primary porosity in sample H-7749 taken from the Hamon #A-3 Humphreys core at a depth of 7749 ft. within DDTB facies. Sample is under 5X magnification in plane polarized light. (H-7749 5X PPL)

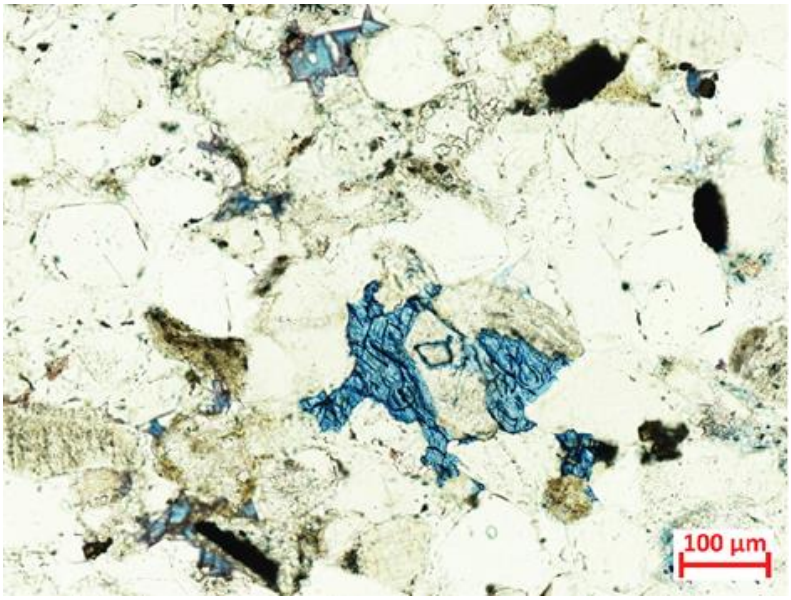

Figure 33: Calcite cement occluding primary porosity in sample H-7691 taken from the Hamon #A-3 Humphreys core at a depth of 7691 ft. within TETB facies. Sample is under 20X magnification in plane polarized light. (H-7691 20X PPL)

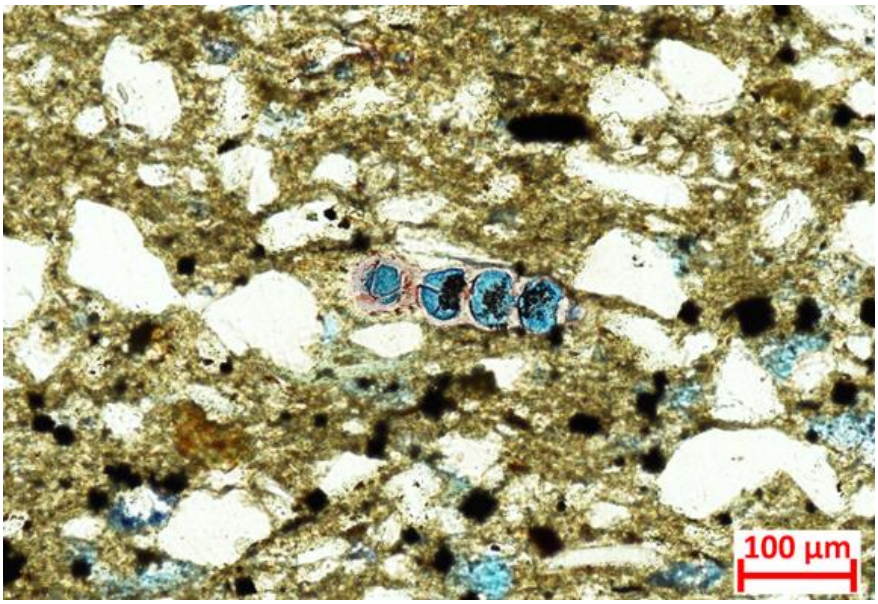

Figure 34: Reophax with secondary porosity in sample L-7632 taken from the Sun #1 Lockhart core at a depth of 7632 ft. within PDTB facies. Sample is under 20X magnification in plane polarized light. (L-7632 20X PPL)

Petrographic Variations Among Facies

The Tonkawa Sandstone displays relatively uniform petrographic qualities among facies. However, minor variability is present. Distal facies such as Distal Shelf (DS), Distal Bioturbated Shelf (DBS), and Distal Deltaic Tidal Bar (DDTB) facies, which have a higher percentage of mud occurring in both thin mud-drapes as well as within the matrix, have a higher percentage of micas and organic matter. Quartz overgrowth commonly occludes primary porosity across each facies, however, minor amounts of secondary porosity occurs in Proximal Deltaic Tidal Bar facies (PDTB) as well as Transgressive Estuarine Tidal Bar facies (TETB).

Chapter 5: Discussion

Cores

Sun #1 Lockhart

The sediments in this core are a part of a tidal bar complex within a tidally influenced estuary or tide dominated delta. Plant and wood fragments were transported from a nearby terrestrial environment. Upper-flow regime planar stratification in the TST-3 interval from 7607-7618 ft. suggests that the interval in this core represents a setting proximal to the mouth of a distributary channel feeding an estuary. Well-developed bidirectional ripple bedforms, rhythmic bedding, double-mud drapes and flaser bedding supports the interpretation of a tidally influenced environment. Double-mud drapes, also known as mud-layer couplets have been interpreted to represent deposition during the two slack-water periods associated with the ebb and flow of dominant and subordinate tidal currents within a complete tidal cycle (Visser, 1980). Mud-layer couplets observed in the TETB facies within this core indicate a shallow, tidally-modified estuarine environment such as that observed along the Netherlands coast by Visser (1980). Additionally, interbedded sandstone and mudstone lithologies throughout the core record fluctuating currents consistent with tidal cycles. HST-3 and TST-3 were deposited in a tide-dominated delta and a tide-dominated estuary, respectively. Distal Bioturbated Shelf (DBS) facies, Distal Deltaic Tidal Bar (DDTB) facies, and Proximal Deltaic Tidal Bar (PDTB) facies occur in HST-3. Transgressive Estuarine Tidal Bar (TETB) facies and Distal Shelf (DS) facies occurs within TST-3.

Internorth #1-46 Humphreys

Facies in this core represents a more distal environment than that of the Sun #1 Lockhart, owing to the high percentage of very fine mudstones and sandstones. The sediments were deposited on the distal portion on the shelf, which is supported by the mud-rich lithology, as well as the starved ripple bedforms and clam burrows. Facies observed within this core include Distal Shelf (DS) facies, Proximal Deltaic Tidal Bar (PDTB) facies, and Distal Deltaic Tidal Bar (DDTB) facies, all of which occur in the HST-3 interval, the only stratigraphic interval present in the core.

Hamon #A-3 Humphreys

Owing to the abundance of clay drapes and ripple bedforms within the core, in conjunction with the wavy and lenticular bedding, deposits in this core are interpreted to have been deposited in a tidal setting, entirely within the subtidal to intertidal zone. No subaerial exposure surfaces were observed. Subaerial exposure surfaces are surfaces of rock that have been exposed at the earth's surface to diagenetic processes that modify or destroy sedimentary fabrics. These surfaces mark a period of non-deposition and often erosion and represent a break in the sedimentary sequence (Esteban and Klappa, 1983). This interval is part of a prograding tidal bar complex within a tide-dominated deltaic setting. The TST-3 interval, because of its retrogradational vertical profile, is interpreted as having been deposited in an estuarine setting. Facies observed within this core include Distal Bioturbated Shelf (DBS) facies and Distal Shelf (DS) facies occur within the TST-2 interval. Proximal Deltaic Tidal Bar (PDTB) facies and Distal Deltaic Tidal Bar (DDTB) facies are observed within the HST-3 interval. Distal

Bioturbated Shelf (DBS) facies and Transgressive Estuarine Tidal Bar (TETB) facies are observed in the TST-3 interval.

Sandstone-Body Distribution

Sandstone-body distribution in the HST-2 interval suggests a deltaic, shallow-marine setting. Dip-elongate sandstone bodies displaying a northeast-southwest orientation suggest distributary channels feeding a delta from the northeast to the southwest. However, the thickest sandstone bodies are distributed along strike by wave energy along the paleoshoreline in a northwest-southeast orientation, such as those observed in the Maastrichtian Fox Hills Formation in the Washakie Basin, Wyoming (Olariu et al., 2012). Sand bodies display a strongly progradational log response observed in wireline log cross sections. For these reasons, the HST-2 interval is interpreted to have been deposited in a mixed fluvial, tide, and wave influenced deltaic environment.

In contrast, the HST-3 interval has markedly different sandstone-body geometries with respect to the HST-2 interval. Sandstone-body geometries in the HST-3 interval are dip-elongate and dip-parallel, displaying dimensions of 3-5 mi. (4.82-8.04 km) in length, and up to 0.5 mi. (0.8 km) in width. Such geometries are consistent with tidal bar complexes within a tide-dominated delta, such as those seen in the Misoa Formation in the Maracaibo Basin (Maguregui, 1990; Maguregui and Tyler, 1991). Wireline log response of these sandstone bodies is strongly progradational and sandier than HST-2, suggesting that the HST-3 interval represents a more proximal environment than that in the HST-2 interval. This stacking pattern is consistent with that of a prograding delta front. Delta-front deposits within a tide-dominated deltaic environment

are often deposited into parallel, upward-coarsening sandstone bodies (Off, 1963; Klein, 1970). The absence of sandstone bodies distributed along the paleoshoreline suggests a significant decrease in wave energy during HST-3 deposition, relative to HST-2. The inferred paleoshoreline displays a northwest-southeast orientation that had migrated slightly southwestward following HST-2 deposition. Thick sandstone bodies northeast of the study area also suggest a northeastern sediment source.

Within the more proximal portion of the study area, TST-3 sandstone bodies are dip-elongate and display morphologies consistent with tidal bar complexes as well as estuarine tidal channel-fill deposits such as those seen in Misoa Formation (Ambrose et al., 1995). In more distal portions of the study area, towards the paleoshoreline, sandstone bodies in TST-3 were distributed along strike by wave energy, as in HST-2. Wireline log responses for sandstone bodies in this interval are retrogradational, suggesting a transgression during TST-3 deposition. Because sandstone bodies in TST-3 were deposited during a transgression and exhibit geometries consistent with tidal bar complexes and estuarine tidal channel-fill deposits, the TST-3 interval has been interpreted as having been deposited in a mixed tide and wave influenced estuarine environment along a transgressive shoreline. Estuarine deposits such as this occur in early highstand and transgressive systems tracts (Dalrymple et al., 1992). Similar to both the HST-2 and HST-3 intervals, the sediment source area is to the northeast.

Implications for Petroleum Exploration and Production

Tonkawa deposits in the southwest portion of the study area, down-dip of the paleoshoreline, are sandstone-poor, and therefore hydrocarbon exploration should focus on the

up-dip Tonkawa trend closer to the source area, in the northeast Hemphill County and southern Lipscomb County. Tonkawa sandstone-body geometries are highly variable within the sequence stratigraphic framework. This variability is most likely attributed to the autocyclic processes such as the alternation between a mixed tide and wave-dominated energy regime and a strictly tide-dominated energy regime. Additionally, differential subsidence within the basin may have attributed to the variance in sandstone-body geometry within individual sequences of deposition.

Efficient exploration and production of hydrocarbons in the Tonkawa Sandstone depends on a detailed understanding of the depositional trends associated with the environment in which each chronostratigraphic interval was deposited. The integration of depositional and reservoir analogs for sandstone-rich intervals of the Tonkawa Sandstone can help optimize hydrocarbon recovery by predicting the size, shape, and location of reservoir rock as well as barriers to flow. Because the Tonkawa Sandstone was deposited in a variety of depositional environments, no single analog can appropriately compare depositional patterns or future reservoir development. Depositional analogs have been chosen for each of the sandstone-rich intervals mapped in the study area: HST-2, HST-3, and TST-3.

HST-2

The HST-2 interval has been interpreted as having been deposited in a mixed tide, fluvial, and wave-influenced deltaic environment. A potential analog for the Tonkawa Sandstone HST-2 interval is the Fox Hills Formation in the Washakie Basin, Wyoming. The Fox Hills Formation was deposited in a mixed fluvial, tide and wave-influenced deltaic environment in which deltas thicken across the shelf and fluvial and tidal energy dominance is replaced by increased wave energy in a basinward direction across the shelf (Olariu et al., 2012). L2 delta lobes within

cyclothem 10 of the Fox Hills Formation display strike-oriented sandstone bodies redistributed by wave energy (Olariu et al., 2012), similar to the geometry of sandstone bodies in the Tonkawa Sandstone HST-2 interval. Additionally, elongate distributaries such as those observed in the HST-2, were serving as conduits for sedimentation to the deltas found in the Fox Hills Formation. Additionally, the Fox Hills Formation serves as a good reservoir analog for the HST-2 interval.

Exploration within HST-2 interval should target elongate, strike-oriented sandstone bodies redistributed by wave energy and longshore drift along a northwest-southeast paleoshoreline. These sandstone bodies will make attractive targets for exploration due to their high degree of continuity. In developing these sand bodies however, one must consider the asymmetric geometry of wave-dominated deltas (Bhattacharya and Giosan, 2003) which result in clean, thick sandstone bodies on the up-drift side of the shoreline and sandstone bodies encased in delta-plain muds on the down-drift side of the shoreline which can act as barriers to flow, limiting reservoir connectivity (Olariu et al., 2012).

HST-3

The Lower Eocene Misoa Formation in the Maracaibo Basin in Venezuela is a depositional analog for the Tonkawa Sandstone HST-3 interval. The Misoa Formation, like the HST-3 interval of the Tonkawa Sandstone, was deposited in a tide-dominated deltaic environment (Figure 35). Sandstone body geometries observed in the Misoa Formation include dip-elongate distributary channel and tidal channel deposits associated with dip-parallel delta front deposits. Additionally, sandstone bodies in the C member of the Misoa Formation are narrow, less than 2,000 ft. (610 m) wide (Ambrose et al., 1995). Similar geometries and

dimensions were observed in sandstone bodies within the HST-3 interval of the Tonkawa Sandstone.

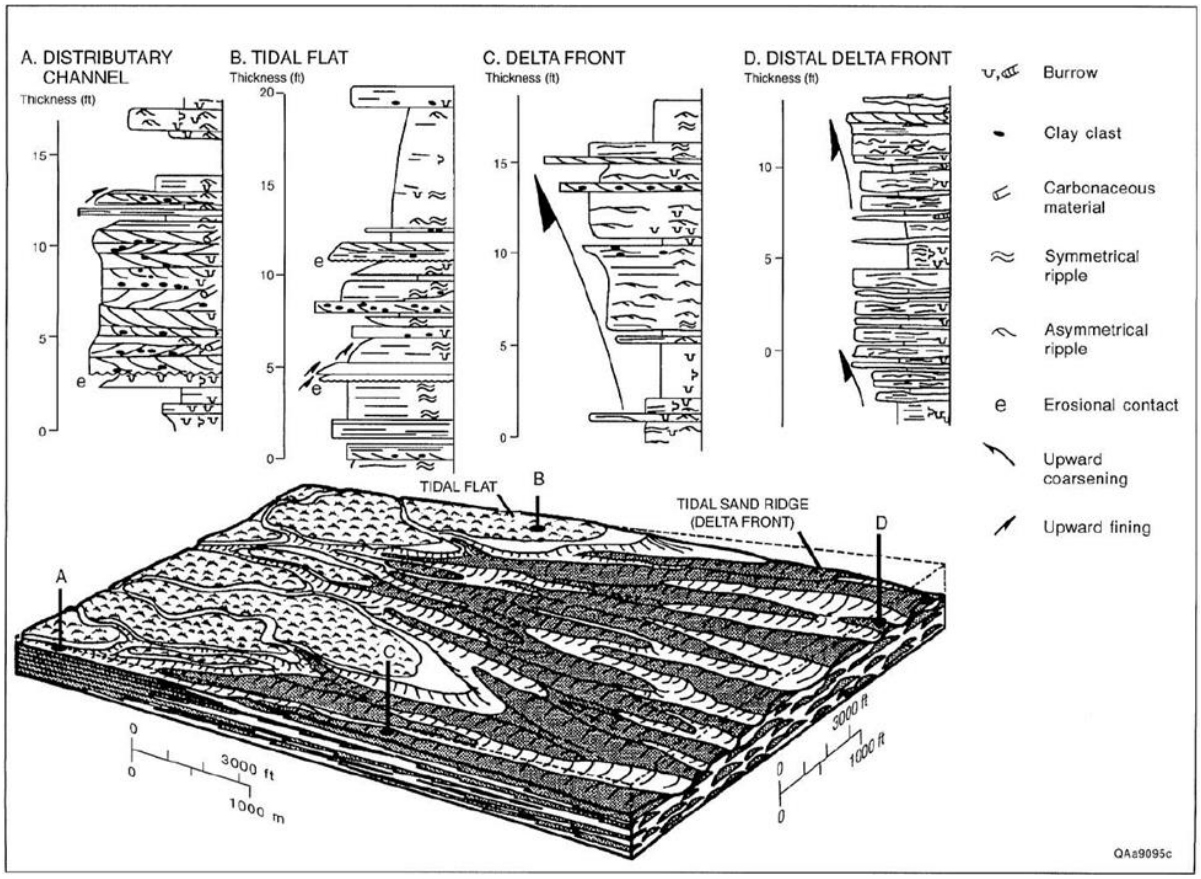

Figure 35: Tide-dominated deltaic depositional model (Ambrose, 1995; modified from Maguregui, 1990).

Similar to the HST-3 interval, sedimentary structures observed in the Misoa Formation include repetitive, clay-draped reactivation surfaces, abundant clay clasts, and bidirectional ripple bedforms. Reactivation surfaces, which consist of flaser ripple bedforms and thin mud layers draping clean sands, are a product of fluctuating energy conditions caused by alternating ebb and flow currents (Reineck and Wunderlich, 1968; Reineck and Singh, 1973). Reactivation

surfaces and clay clasts found in core were interpreted to have been the result of scouring of a mud-rich substrate by tidal currents (Ambrose et al., 1995). While bidirectional ripple bedforms were observed in the Misoa Formation, they were relatively uncommon. The rarity of bidirectional ripple bedforms has been attributed to a dominant tidal current which resulted in the preferential preservation of unidirectional bedforms (Ambrose et al., 1995). This interpretation has been employed for the cores within this study as well. While bidirectional ripple bedforms were observed in cores such as the Sun #1 Lockhart, they were relatively uncommon compared to other sedimentary structures.

Tide-dominated deltaic reservoirs such as the Misoa Formation, as well as the HST-3 interval of the Tonkawa Sandstone, are commonly characterized by dip-elongate, dip-parallel delta-front sandstones. Exploration in the HST-3 interval should target dip-elongate sandstone bodies with a northeast-southwest orientation. Additionally, tide-dominated deltaic reservoirs such as the Tonkawa Sandstone and the Misoa Formation commonly contain interbedded sandstones and mudstones. The high degree of heterogeneity associated with these heterolithic deposits leads to both high volumes of unproduced oil within the reservoir as well as the associated potential for secondary oil recovery (Ambrose et al., 1995).

TST-3

The Lower Cretaceous Viking Formation, within the Crystal-Viking Filed in Alberta, Canada serves as a good depositional and reservoir analog for the TST-3 interval of the Tonkawa Sandstone. The Crystal Viking Formation has been interpreted as having been deposited in a tide-influenced estuarine environment along a transgressive shoreline (Reinson et al., 1988). The Viking Formation is characterized by linear sandstone bodies, up to 30 meters thick that have

been interpreted as multistage tidal channel-fill complex deposits, unconformably overlying shoreface facies (Reinson et al., 1988). Linear sandstone bodies in the TST-3 interval have been interpreted to have been deposited in an estuarine tidal bar complex, similar to that of the Viking Formation.

Additionally, fluvial-estuarine channel deposits observed in the Misoa Formation may serve as a good depositional analog for the TST-3 interval of the Tonkawa Sandstone. In the Lower C-6-X submember of the Misoa Formation, permeability values are highest at the base of upward-fining, retrogradational intervals consisting of unburrowed sandstones with tabular crossbeds at the base which are overlain by sandstones with ripples and plane beds. An increase in clay clasts and organic fragments were also observed up-section in these upward-fining intervals. Similarly, within the TST-3 interval permeability values are highest at the base of Transgressive Estuarine Tidal Bar (TETB) facies (Figure 15) which commonly consist of unburrowed sandstones at the base overlain finer-grained sediments with an increase in clay clasts up-section (Figure 15).

Exploration in the TST-3 interval should target estuarine tidal-channel sandstone bodies displaying an east-west orientation within the eastern portion of the study area. Additionally, to the west, wave-reworked sandstone bodies with an elongate geometry and a northwest-southeast orientation may contain potential reservoir rock.

Reservoir Quality Within Facies

Despite widespread quartz overgrowths as well as calcite cement occluding primary porosity in more proximal facies, variation in reservoir quality among facies does exist. Porosity and permeability values are greater in proximal facies such as PDTB and TETB facies. This is

attributed to larger grain size and better sorting than observed in more distal facies, such as the DDTB facies, which is characterized by increased mud and clay content in sandstone beds as well as within the matrix, commonly filling pore spaces. Additionally, PDTB facies as well as TETB facies to a lesser, extent are less heterolithic than the DDTB facies. PDTB and TETB facies display significantly fewer mud drapes and less wavy, lenticular and flaser bedding, which would consequently yield greater vertical permeability through the reservoir. The most distal facies (DS and DBS) display the worst reservoir quality. Significant primary or secondary porosity is absent in these facies, with only microporosity present. Because of the low permeability of the Tonkawa Sandstone, attributed mainly to widespread quartz overgrowth combined with the fine-grained nature of the sediments, a stimulation method such as hydraulic fracturing would be beneficial to increase reservoir connectivity.

Chapter 6: Conclusions

The late Pennsylvanian Tonkawa Sandstone in the western Anadarko Basin was deposited primarily in deltaic and estuarine environments with a source area to the northeast. The HST-2 interval, the oldest sandstone-rich sequence of deposition in the Tonkawa Sandstone, was deposited in a deltaic environment with a mixed wave and tide-dominated energy regime. The younger HST-3 interval was deposited in a tide-dominated deltaic environment. The TST-3 interval, the youngest sandstone-rich sequence of deposition of the Tonkawa Sandstone, was deposited in a transgressive estuarine environment. The Tonkawa Sandstone represents three relatively high-order transgressive-regressive sequences, encompassed by one larger lower-order sequence. Sandstone body geometries vary greatly within the stratigraphic framework.

The Tonkawa Sandstone is a fine-grained litharenite to sublitharenite rich in metamorphic rock fragments. Across facies, samples vary slightly in mineralogy with more distal mud-rich facies such as Distal Bioturbated Shelf (DBS) and Distal Shelf (DS) being more mud-rich in micas, organic matter and mud. More proximal facies such as Proximal Deltaic Tidal Bar (PDTB) and Transgressive Estuarine Tidal Bar (TETB) are commonly more porous and permeable than distal facies, a result of larger grain size and better sorting. However, owing to widespread quartz overgrowths, variation in reservoir quality is relatively limited.

Successful exploration within the Tonkawa Sandstone relies heavily on an understanding of the depositional environment in which each chronostratigraphic interval was deposited. Within the HST-2 interval, potential reservoirs are strike-elongate, strike-oriented sandstone bodies that were redistributed by wave energy along a northwest-southeast trending

paleoshoreline. Optimal reservoirs within this interval can be expected to occur on the up-drift side of the shoreline due to the asymmetry of wave-dominated deltas (Bhattacharya, 2003). Exploration within the HST-3 interval should target dip-elongate, dip-parallel tidal bar sandstone bodies with a northeast-southwest orientation. The high degree of heterogeneity associated with tide-dominate deltaic reservoirs such as the HST-3 interval may result in high volumes of unproduced oil within the reservoir, allowing for potential secondary oil recovery operations. Exploration within the TST-3 interval should target the base of fining-upward tidal-channel sandstone bodies with an east-west orientation, in which permeability values and presumed reservoir quality is the highest. To the west, elongate, wave-reworked TST-3 sandstone bodies with a northwest-southeast orientation may also contain potential reservoir rock, similar to the sandstone bodies observed along strike in the HST-2 interval.

In conclusion, detailed analysis of Pennsylvanian formations such as the Tonkawa Sandstone can aid in the characterization of other Pennsylvanian strata within the Anadarko Basin, as well as other foreland and cratonic basins worldwide.

Appendix

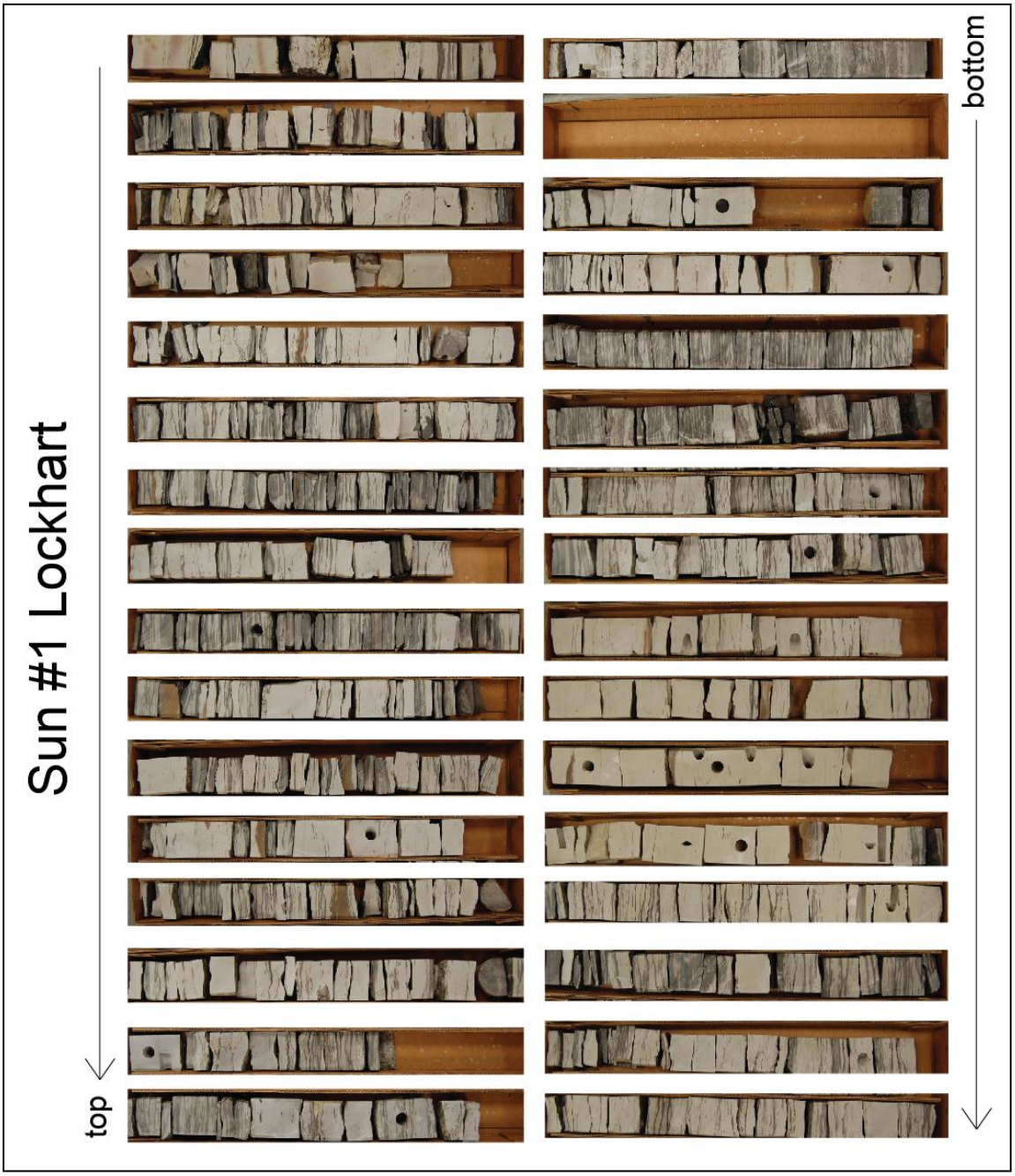

Figure 36: Sun #1 Lockhart core

Figure 37: Internorth #1-46 Humphreys core

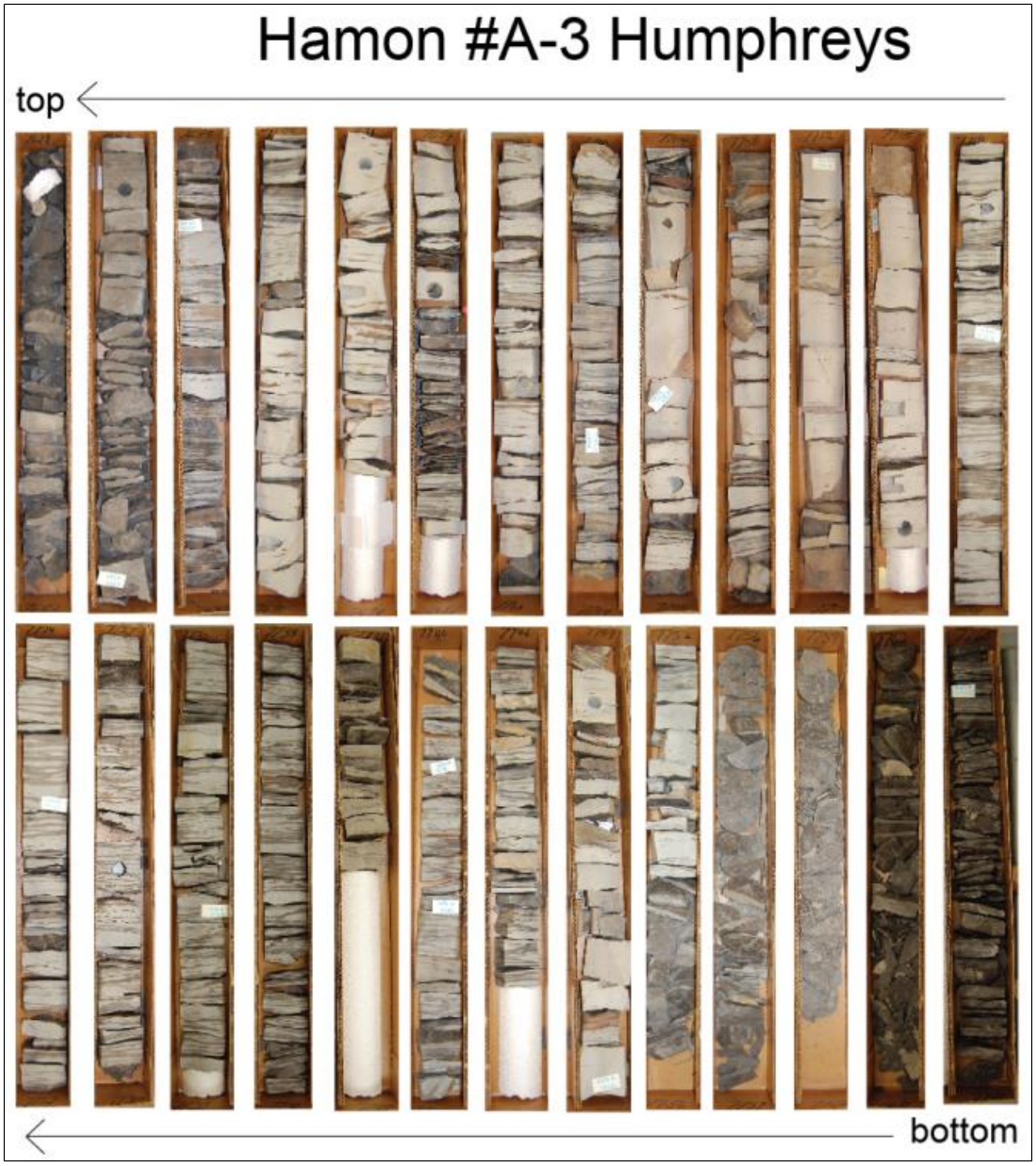

Figure 38: Hamon #A-3 Humphreys core

SAMPLE	QUARTZ	FELDSPARS	LITHICS
	%	%	%
H-7682	69.00%	0.00%	31.00%
H-7691	83.00%	0.00%	16.00%
H-7718	68.00%	1.00%	31.00%
H-7728	74.00%	1.00%	25.00%
H-7749	81.00%	0.00%	19.00%
L-7580	81.00%	0.00%	19.00%
L-7622	70.00%	0.00%	30.00%
L-7632	63.00%	1.00%	37.00%
L-7649	76.00%	0.00%	24.00%
I-7670	75.00%	0.00%	25.00%
I-7675	76.00%	1.00%	23.00%
I-7678	63.00%	0.00%	37.00%
I-7678.5	68.00%	1.00%	31.00%
I-7698	71.00%	0.00%	29.00%
I-7702.5	72.00%	0.00%	28.00%
I-7705.5	66.00%	0.00%	34.00%
Averages:	72.25%	0.31%	27.44%

Table 3: Normalized percentages of quartz, feldspars, and lithics in thin sections

Permeability Values within the HST-3 Interval					
Hamon #A-3 Humphries		Sun #1 Lockhart		Internorth #1-46 Humphreys	
Depth	K (mD)	Depth	K (mD)	Depth	K (mD)
7716.0372	2.5	7621.088	1.89	7666.7797	0.238
7716.037	1.95	7621.087	1.9	7666.874	1.88
7716.8238	1.44	7621.481	2.58	7667.0427	5.92
7716.9545	1.42	7621.753	5.95	7667.1952	4.81
7717.1365	1.57	7621.769	5.85	7667.6339	0.894
7717.3002	1.31	7622.145	2.87	7667.8358	0.464
7717.4991	1.19	7622.496	2.4	7668.0852	1.16
7717.677	1.88	7622.71	1.32	7668.2026	0.674
7717.7016	0.702	7623.21	2.34	7668.5947	1.2
7718.0606	0.941	7623.36	1.73	7668.8317	0.588
7718.0865	0.759	7624.098	2.61	7669.0108	1.22
7718.2416	0.514	7624.56	1.1	7669.8022	0.136
7718.5084	2.04	7624.819	1.88	7670.2698	0.758
7718.6091	2.44	7625.038	1.6	7670.4288	0.331
7718.8215	1.01	7625.419	0.972	7670.7825	0.301
7719.1736	0.504	7625.837	0.963	7671.0562	1.4
7719.3595	0.449	7626.003	1.31	7671.1818	1.31
7719.6976	0.555	7626.436	1.05	7671.2984	0.33
7719.9653	0.419	7627.124	1.36	7671.639	0.301
7720.233	1.35	7627.528	0.573	7671.7693	1.63
7720.3497	0.379	7627.873	1.21	7672.0566	0.545
7720.5896	0.604	7628.078	1.17	7672.5363	3.53
7720.7604	0.379	7628.656	1.24	7672.9002	1.69
7720.8675	0.49	7629.098	0.749	7673.0938	0.977
7724.1746	0.311	7629.475	1.12	7673.2134	0.381
7724.3322	0.237	7630.127	0.757	7673.5679	0.255
7724.5735	0.48	7630.544	0.362	7673.6942	5.98
7724.8106	0.485	7630.838	0.359	7674.2329	1.43
7725.1034	0.327	7631.146	0.728	7674.5907	0.452
7725.414	0.552	7631.43	0.902	7674.8429	0.782
7725.5715	0.396	7631.826	0.602	7675.4058	4.96
7726.082	1.3	7632.224	0.34	7675.514	0.294
7726.6642	0.445	7632.452	0.355	7675.7347	1.25
7727.9854	0.325	7632.738	1.12	7675.9514	2.35
7728.2466	0.786	7633.202	0.393	7676.2355	3.29
7728.6	23.4	7633.548	0.637	7676.7931	0.464
7728.743	7.35	7633.848	1.22	7677.0585	2.53
7728.9791	22.9	7634.17	0.561	7677.3079	0.811
7729.1027	4.95	7634.499	0.602	7677.5282	0.456
7730.0195	0.725	7634.921	0.376	7677.8101	0.21
7730.2381	0.363	7635.149	0.445	7678.1182	0.962
7730.3321	0.577	7635.576	0.592	7678.3626	0.266

7730.7683	0.313	7635.764	0.221	7678.5756	1.31
7730.9744	0.284	7636.637	2.93	7679.0017	2.6
7731.2828	1.16	7636.937	0.66	7679.2855	0.546
7731.705	0.492	7637.338	0.68	7679.694	0.681
7732.1248	0.71	7637.549	0.341	7680.1806	0.973
7732.4226	0.514	7638.039	0.514	7680.31	2.63
7732.5758	1.17	7638.527	0.667	7680.557	0.287
7732.7148	1.54	7639.863	0.317	7681.05	1.03
7733.1599	0.987	7640.257	0.32	7681.5348	0.445
7733.638	3.09	7641.046	0.303	7681.8046	2.36
7734.0696	0.931	7641.444	0.872	7683.1454	1.53
7734.227	0.916	7641.685	1.82	7683.3588	0.274
7734.3927	1.28	7641.685	0.888	7684.5773	0.689
7734.7175	0.43	7642.108	0.4	7684.6996	1.4
7734.8493	0.388	7642.298	1.29	7684.9323	1.39
7735.1044	0.836	7642.726	1.13	7685.5494	0.512
7735.3351	1.24	7642.962	1.13	7685.8747	10.9
7735.5203	33.6	7643.252	0.838	7686.2374	2.62
7740.1368	1.17	7643.6	1.21	7686.9581	4.38
7740.4735	2.14	7643.927	2.21	7687.635	0.73
7740.8593	1.78	7643.927	3.27	7688.3675	4.94
7740.9914	0.287	7644.25	0.841	7688.7452	1.29
7741.6437	0.419	7644.629	0.999	7689.6434	0.755
7741.8262	1.76	7644.879	0.844	7689.8587	1.31
7742.3557	2.69	7648.214	0.732	7690.7955	0.731
7746.109	0.505	7648.606	0.65	7691.2785	0.664
7746.8272	7.42	7648.929	0.453	7692.5425	1.25
7747.1567	0.814	7649.138	0.79	7692.8473	1.65
7747.6257	1.65	7649.342	1.66	7693.1053	0.468
7747.8725	5.92	7654.068	0.225	7693.5595	0.473
7749.1237	1.33	7654.357	0.335	7693.7329	0.496
7749.3515	11.9	7654.774	0.399	7693.9493	0.808
7749.6941	1.34	7655.302	0.884	7694.3103	5.86
7749.93	1.29	7655.538	0.315	7694.5609	2.23
7750.0396	0.923	7655.822	0.709	7694.5642	1.25
7750.1972	1.29	7656.374	0.79	7694.5739	2.18
7750.3283	0.731	7656.883	0.477	7694.9302	0.522
7750.5277	3.61			7695.1977	0.984
7750.8685	0.653			7695.4079	0.291
7751.0708	1.25			7695.6856	1.65
7751.3032	1.45			7695.787	0.281
7751.5437	0.687			7696.0473	3.7
7751.6824	0.872			7696.0521	2.35

7752.0099	1.71			7696.5414	5.14
7752.5858	0.52			7696.5421	6.13
7752.9316	0.567			7696.9589	3.86
7753.1214	1.32			7697.1937	0.401
7753.5439	0.0955			7697.4064	0.684
7753.7019	0.462			7697.692	0.95
				7698.0533	0.411
				7698.367	0.634
				7698.7195	0.755
				7699.0219	0.335
				7699.0246	0.886
				7699.2768	0.729
				7699.5822	0.494
				7699.8412	0.511
				7700.2828	0.63
				7700.5373	0.63
				7700.8641	5.79
				7701.0155	0.834
				7701.423	0.478
				7701.6257	2.15
				7701.6712	0.381
				7701.9097	0.427
				7702.0739	0.433
				7702.5392	0.513
				7703.0318	1.17
				7703.6985	0.639
				7703.8198	0.758
				7704.4111	0.443
				7704.7556	0.591
				7704.9501	5.13
				7704.9604	4.14
				7705.0696	0.423
				7705.224	0.903
				7705.5628	0.57
				7705.9068	0.455
				7705.9074	4.66
				7706.3069	1.18
				7706.9019	0.516
				7707.1987	1.02
				7707.5998	3.06
				7709.2442	0.92
				7709.7674	4.68
Average:	2.210335165	Average:	1.15446	Average:	1.561212598

Table 4: Minipermeameter-derived permeability values within the HST-3 interval

Hamon #A-3 Humphreys Minipermeameter Data																			
Depth	K (mD)	Depth	K (mD)	Depth	K (mD)	Depth	K (mD)	Depth	K (mD)	Depth	K (mD)	Depth	K (mD)	Depth	K (mD)	Depth	K (mD)	Depth	K (mD)
7682.061	1.14	7689.871	0.927	7699.124	1.21	7708.148	1.44	7717.137	1.57	7728.6	23.4	7742.356	2.69						
7682.205	1.63	7690.337	0.351	7699.336	0.818	7708.369	2.54	7717.3	1.31	7728.743	7.35	7746.109	0.505						
7682.421	1.29	7690.607	0.702	7699.443	2.2	7708.6	0.248	7717.499	1.19	7728.979	22.9	7746.827	7.42						
7682.548	1.35	7691.072	0.93	7699.608	0.262	7708.991	0.339	7717.677	1.88	7729.103	4.95	7747.157	0.814						
7682.799	6.49	7691.356	0.518	7700.055	0.311	7709.172	0.366	7717.702	0.702	7730.02	0.725	7747.626	1.65						
7682.889	2.03	7691.508	0.873	7700.18	3.08	7709.25	1.12	7718.061	0.941	7730.238	0.363	7747.873	5.92						
7683.056	1.28	7691.842	0.539	7700.451	0.478	7709.356	0.881	7718.087	0.759	7730.332	0.577	7749.124	1.33						
7683.332	1.24	7692.116	0.613	7700.551	0.311	7709.751	0.525	7718.242	0.514	7730.768	0.313	7749.352	11.9						
7685.066	0.249	7692.392	9.8	7700.649	0.422	7710.064	0.491	7718.508	2.04	7730.974	0.284	7749.694	1.34						
7685.581	0.139	7692.389	5.23	7700.968	1.17	7712.097	0.755	7718.609	2.44	7731.283	1.16	7749.93	1.29						
7685.663	0.137	7692.498	0.332	7701.143	0.858	7712.192	0.605	7718.822	1.01	7731.705	0.492	7750.04	0.923						
7685.863	0.382	7692.973	0.251	7701.825	2.43	7712.394	0.374	7719.174	0.504	7732.125	0.71	7750.197	1.29						
7686.047	0.374	7693.134	1.21	7701.926	0.891	7712.575	0.413	7719.36	0.449	7732.423	0.514	7750.328	0.731						
7686.281	0.158	7693.134	0.668	7702.056	0.486	7712.796	0.674	7719.698	0.555	7732.576	1.17	7750.528	3.61						
7686.317	2.16	7693.484	0.404	7702.492	2.6	7712.925	0.647	7719.965	0.419	7732.715	1.54	7750.869	0.653						
7686.52	0.534	7694.107	0.517	7702.498	1.09	7713.014	0.659	7720.233	1.35	7733.16	0.987	7751.071	1.25						
7686.82	1.36	7694.437	0.872	7702.609	0.751	7713.082	0.825	7720.35	0.379	7733.638	3.09	7751.303	1.45						
7687.013	0.179	7695.082	0.306	7702.835	0.303	7713.168	1.09	7720.59	0.604	7734.07	0.931	7751.544	0.687						
7687.346	4.45	7695.211	1.17	7704.172	1.46	7713.372	0.379	7720.76	0.379	7734.227	0.916	7751.682	0.872						
7687.34	4.96	7696.066	0.499	7704.327	0.649	7713.552	2.39	7720.868	0.49	7734.393	1.28	7752.01	1.71						
7687.418	1.36	7696.317	0.227	7704.556	0.996	7713.845	2.27	7724.175	0.311	7734.718	0.43	7752.586	0.52						
7687.532	0.254	7696.465	0.289	7704.84	1.35	7714.237	0.548	7724.332	0.237	7734.849	0.388	7752.932	0.567						
7687.703	1.18	7697.078	0.722	7705.045	0.664	7714.531	0.414	7724.574	0.48	7735.104	0.836	7753.121	1.32						
7688.158	0.179	7697.213	0.374	7705.461	1.23	7714.618	1.26	7724.811	0.485	7735.335	1.24	7753.544	0.0955						
7688.23	8.03	7697.376	0.271	7705.538	1.49	7715.354	0.794	7725.103	0.327	7735.52	33.6	7753.702	0.462						
7688.42	6.97	7697.598	0.45	7705.761	0.714	7715.676	1.05	7725.414	0.552	7740.137	1.17								
7688.785	0.354	7697.689	3.15	7705.893	1.17	7715.853	1.29	7725.572	0.396	7740.474	2.14								
7688.963	0.301	7698.018	0.493	7706.098	0.656	7716.037	2.5	7726.082	1.3	7740.859	1.78								
7689.172	0.258	7698.493	0.215	7706.467	1.07	7716.037	1.95	7726.664	0.445	7740.991	0.287								
7689.454	0.347	7698.665	0.25	7708.074	12.5	7716.824	1.44	7727.985	0.325	7741.644	0.419								
7689.618	0.519	7698.868	0.693	7708.155	2.1	7716.955	1.42	7728.247	0.786	7741.826	1.76								

Table 5: Hamon #A-3 Humphreys minipermeameter data

Internorth #1-46 Humphreys Minipermeameter Data									
Depth	K (mD)	Depth	K (mD)	Depth	K (mD)	Depth	K (mD)	Depth	K (mD)
7666.78	0.238	7675.514	0.294	7688.368	4.94	7698.72	0.755	7707.6	3.06
7666.874	1.88	7675.735	1.25	7688.745	1.29	7699.022	0.335	7709.244	0.92
7667.043	5.92	7675.951	2.35	7689.643	0.755	7699.025	0.886	7709.767	4.68
7667.195	4.81	7676.236	3.29	7689.859	1.31	7699.277	0.729		
7667.634	0.894	7676.793	0.464	7690.796	0.731	7699.582	0.494		
7667.836	0.464	7677.059	2.53	7691.279	0.664	7699.841	0.511		
7668.085	1.16	7677.308	0.811	7692.543	1.25	7700.283	0.63		
7668.203	0.674	7677.528	0.456	7692.847	1.65	7700.537	0.63		
7668.595	1.2	7677.81	0.21	7693.105	0.468	7700.864	5.79		
7668.832	0.588	7678.118	0.962	7693.56	0.473	7701.016	0.834		
7669.011	1.22	7678.363	0.266	7693.733	0.496	7701.423	0.478		
7669.802	0.136	7678.576	1.31	7693.949	0.808	7701.626	2.15		
7670.27	0.758	7679.002	2.6	7694.31	5.86	7701.671	0.381		
7670.429	0.331	7679.286	0.546	7694.561	2.23	7701.91	0.427		
7670.783	0.301	7679.694	0.681	7694.564	1.25	7702.074	0.433		
7671.056	1.4	7680.181	0.973	7694.574	2.18	7702.539	0.513		
7671.182	1.31	7680.31	2.63	7694.93	0.522	7703.032	1.17		
7671.298	0.33	7680.557	0.287	7695.198	0.984	7703.699	0.639		
7671.639	0.301	7681.05	1.03	7695.408	0.291	7703.82	0.758		
7671.769	1.63	7681.535	0.445	7695.686	1.65	7704.411	0.443		
7672.057	0.545	7681.805	2.36	7695.787	0.281	7704.756	0.591		
7672.536	3.53	7683.145	1.53	7696.047	3.7	7704.95	5.13		
7672.9	1.69	7683.359	0.274	7696.052	2.35	7704.96	4.14		
7673.094	0.977	7684.577	0.689	7696.541	5.14	7705.07	0.423		
7673.213	0.381	7684.7	1.4	7696.542	6.13	7705.224	0.903		
7673.568	0.255	7684.932	1.39	7696.959	3.86	7705.563	0.57		
7673.694	5.98	7685.549	0.512	7697.194	0.401	7705.907	0.455		
7674.233	1.43	7685.875	10.9	7697.406	0.684	7705.907	4.66		
7674.591	0.452	7686.237	2.62	7697.692	0.95	7706.307	1.18		
7674.843	0.782	7686.958	4.38	7698.053	0.411	7706.902	0.516		
7675.406	4.96	7687.635	0.73	7698.367	0.634	7707.199	1.02		

Table 6: Internorth #1-46 Humphreys minipermeameter data

Sun #1 Lockhart Minipermeameter Data											
Depth	K (mD)	Depth	K (mD)	Depth	K (mD)	Depth	K (mD)	Depth	K (mD)	Depth	K (mD)
7558.169	1.03	7575.493	0.412	7595.2	0.425	7611.146	0.753	7625.419	0.972	7643.6	1.21
7558.448	0.135	7575.81	0.851	7595.547	0.215	7611.388	0.615	7625.837	0.963	7643.927	2.21
7558.996	0.156	7576.308	0.152	7595.942	0.209	7611.736	0.28	7626.003	1.31	7643.927	3.27
7559.135	0.362	7576.636	0.222	7596.206	0.398	7612.183	0.238	7626.436	1.05	7644.25	0.841
7559.517	0.116	7576.824	0.658	7596.451	0.337	7612.69	0.92	7627.124	1.36	7644.629	0.999
7559.927	0.152	7577.179	0.482	7597.349	0.389	7612.812	1.22	7627.528	0.573	7644.879	0.844
7560.162	0.265	7577.47	0.562	7597.601	0.414	7613.233	0.639	7627.873	1.21	7648.214	0.732
7560.426	0.202	7577.85	0.405	7597.986	0.313	7613.56	0.483	7628.078	1.17	7648.606	0.65
7561.057	0.168	7578.184	0.416	7598.175	0.275	7613.984	0.309	7628.656	1.24	7648.929	0.453
7561.555	0.321	7581.417	0.256	7598.467	0.37	7614.292	0.372	7629.098	0.749	7649.138	0.79
7561.854	0.167	7581.878	0.567	7598.875	0.239	7614.73	0.582	7629.475	1.12	7649.342	1.66
7562.031	0.114	7582.097	0.201	7599.199	0.207	7615.233	0.544	7630.127	0.757	7654.068	0.225
7562.661	0.433	7582.504	0.398	7599.401	0.24	7615.474	0.539	7630.544	0.362	7654.357	0.335
7564.025	0.274	7582.881	1.03	7599.561	0.792	7615.923	0.848	7630.838	0.359	7654.774	0.399
7564.532	0.224	7583.029	0.265	7600.364	0.493	7616.48	0.931	7631.146	0.728	7655.302	0.884
7564.852	0.202	7583.68	0.405	7600.584	0.622	7616.784	0.719	7631.43	0.902	7655.538	0.315
7565.018	0.286	7583.918	0.202	7600.884	0.183	7617.11	1.24	7631.826	0.602	7655.822	0.709
7565.462	0.433	7584.295	0.337	7601.136	0.273	7617.523	2.05	7632.224	0.34	7656.374	0.79
7565.718	0.31	7585.176	0.325	7601.523	0.149	7617.519	2.28	7632.452	0.355	7656.883	0.477
7566.083	0.381	7585.487	0.252	7601.912	0.152	7617.521	1.9	7632.738	1.12		
7566.318	0.485	7585.749	0.228	7602.156	0.172	7617.794	2.93	7633.202	0.393		
7566.714	0.439	7586.011	0.259	7602.614	0.634	7617.793	2.37	7633.548	0.637		
7567.198	0.815	7586.735	0.275	7602.876	1.05	7617.899	1.52	7633.848	1.22		
7567.505	0.275	7586.929	8.51	7603.086	0.297	7618.059	4.82	7634.17	0.561		
7567.783	1.21	7586.929	13.2	7603.652	0.293	7618.059	5.68	7634.499	0.602		
7568.144	0.427	7586.964	0.309	7603.955	0.255	7618.253	4.15	7634.921	0.376		
7568.567	0.47	7587.538	0.292	7604.055	0.337	7618.527	4.34	7635.149	0.445		
7568.838	0.303	7588.075	0.219	7604.632	1.54	7619.071	5.28	7635.576	0.592		
7569.183	0.45	7588.503	0.318	7604.623	0.58	7619.669	10.3	7635.764	0.221		
7569.295	0.393	7588.763	0.225	7604.879	0.472	7619.709	8.63	7636.637	2.93		
7569.585	0.434	7589.546	0.297	7605.111	0.742	7620.188	2.79	7636.937	0.66		
7570.151	0.198	7590.002	0.293	7605.567	0.853	7620.561	0.638	7637.338	0.68		
7570.52	0.318	7590.562	0.431	7606.306	0.634	7621.088	1.89	7637.549	0.341		
7570.814	0.438	7590.863	0.352	7606.624	0.574	7621.087	1.9	7638.039	0.514		
7571.121	0.34	7591.18	0.416	7606.855	0.583	7621.481	2.58	7638.527	0.667		
7571.519	0.224	7591.605	0.311	7607.275	0.677	7621.753	5.95	7639.863	0.317		
7571.846	0.278	7591.914	1.02	7607.594	0.587	7621.769	5.85	7640.257	0.32		
7572.118	0.266	7592.236	0.577	7607.815	0.644	7622.145	2.87	7641.046	0.303		
7572.465	0.239	7592.816	0.658	7608.186	1.04	7622.496	2.4	7641.444	0.872		
7573.08	0.259	7593.212	1.23	7608.528	0.496	7622.71	1.32	7641.685	1.82		
7573.637	0.44	7593.567	1.82	7608.644	1.07	7623.21	2.34	7641.685	0.888		
7573.889	1.05	7593.734	0.356	7609.333	0.326	7623.36	1.73	7642.108	0.4		
7574.228	0.765	7593.949	0.299	7609.82	0.473	7624.098	2.61	7642.298	1.29		
7574.507	0.702	7594.069	0.77	7610.092	0.242	7624.56	1.1	7642.726	1.13		
7574.956	1.93	7594.513	0.953	7610.433	0.243	7624.819	1.88	7642.962	1.13		
7575.105	0.436	7594.846	0.499	7610.963	1.06	7625.038	1.6	7643.252	0.838		

Table 7: Sun #1 Lockhart minipermeameter data

References

Ambrose, W.A., Ferrer, E.R., Dutton, S.P., Wang, F.P., Padron, A., Carrasquel, W., Yeh, J.S., and Tyler N., 1995, Production optimization of tide-dominated deltaic reservoirs of the lower Misoa Formation (lower Eocene), LL-652 area, Lagunillas field, Lake Maracaibo, Venezuela: University of Texas at Austin, Bureau of Economic Geology, Report of Investigations 226, 46 p.

Andrews, R.D., 1997, Fluvial-Dominated deltaic (FDD) oil reservoirs in Oklahoma: Oklahoma Geological Survey, Special Publication 97-3, p. 1-11.

Bhattacharya, J. P., and Giosan, L., 2003, Wave-influenced deltas: Geomorphological implications for facies reconstruction: Sedimentology, v. 50, p. 187–210, doi:10.1046/j.1365-3091.2003.00545.x

Billingsley, L. T., and Draves, D. A., 1988, Detailed reservoir analysis of Tonkawa Sandstone (Pennsylvanian) in Bechthold-Frass Field Extension, Texas panhandle area.

Brown, L. F., and Fisher, W. L., 1977, Seismic-stratigraphic interpretation of depositional systems: examples from Brazil rift and pull-apart basins, in Payton, C. E., ed., Seismic Stratigraphy—Applications to Hydrocarbon Exploration: American Association of Petroleum Geologists Memoir 26, p. 213-248.

Cashman, A. L., 2011, Depositional Environment Analysis of the Pennsylvanian, Mid-continent Tonkawa Sandstone: Kansas State University, Master's thesis.

Catuneanu, O., Abreu, V., Bhattacharya, J. P., Blum, M. D., Dalrymple, R. W., Eriksson, P. G., and Winker, C., 2009, Towards the standardization of sequence stratigraphy. Earth-Science Reviews, 92(1), 1-33.

Catuneanu, O., 2006, Principles of sequence stratigraphy. Elsevier.

Clark, G.C., and Aurin, F.L., 1924, The Tonkawa field, Oklahoma: American Association of Petroleum Geologists, v. 8, no. 3, p. 269-283.

Cunningham, B. J., 1961, Stratigraphy Oklahoma-Texas Panhandles.

Dalrymple, R. W., Zaitlin, B. A., and Boyd, R., 1992, Estuarine facies models: conceptual basis and stratigraphic implications: perspective. Journal of Sedimentary Research, 62(6).

Ehrenberg, S. N., et al. "Porosity-permeability relationships in interlayered limestone-dolostone reservoirs." AAPG Bulletin 90.1 (2006): 91-114.

Emery A. F., 2002, Transgressive-Regressive (T-R) Sequence stratigraphy in proceedings of the 22nd Annual Bob F. Perkins Research Conference, Society for Sedimentary Geology, p. 151-172.

Esteban, M., and Klappa, C. F., 1983, Subaerial Exposure Environment, p. 1-22.

Fies, M.W., 1988, Depositional environments and diagenesis of Tonkawa format (Virgilian) in Woods and parts of Woodward Counties, Oklahoma: Oklahoma State University, Master's thesis.

Folk, R. L., 1980, Petrology of sedimentary rocks. Hemphill Publishing Company.

Forchheimer, P., 1901, Wasserbewegung durch Bodem. Zeitschrift Des Vereines Deutscher Ingenieure, v. 45, p. 1782–1788.

Higley, D.K., 2014, Petroleum systems and assessment of undiscovered oil and gas in the Anadarko Basin Province, Colorado, Kansas, Oklahoma, and Texas—USGS Province 58: U.S. Geological Survey Digital Data Series DDS–69–EE, 327 p., 8 pls., http://dx.doi.org/10.3133/ds69EE.

Huang, H., and Ayoub, J., 2006, Applicability of the Forchheimer equation for non-darcy flow in porous media: Society of Petroleum Engineers, SPE 102715, 14 p.

Khaiwka, M. H., 1968, Geometry and depositional environment of Pennsylvanian Sandstones in Northwestern Oklahoma: University of Oklahoma, Doctoral dissertation.

Klein, G., 1970, Depositional and dispersal dynamics of intertidal sand bars: Journal of Sedimentary Petrology, V. 40, p. 1095-11 27.

Kumar, N., and Slatt, R.M., 1984, Submarine-fan and slope facies of Tonkawa (Missourian-Virgilian) Sandstone in deep Anadarko Basin: AAPG Bulletin, v. 68, no. 12, p. 1834-1856.

Maguregui, J. A., and Tyler, N., 1991, Evolution of middle Eocene tide-dominated deltaic sandstones, Lagunillas field, Maracaibo Basin, western Venezuela, in Miall, A. D., and Tyler, Noel, eds., The three-dimensional facies architecture of terrigenous clastic sediments and its implications for hydrocarbon discovery and recovery: SEPM (Society for Sedimentary Geology), v. 3, Concepts in Sedimentology and Paleontology, p. 233-244.

Maguregui, J. A., 1990, Evolution and reservoir properties of middle Eocene tide-dominated deltaic sandstones in eastern Lagunillas field, Maracaibo Basin, Venezuela: The University of Texas at Austin, Master's thesis, 171 p.

Moore, G. E., 1979, Pennsylvanian paleogeography of the southern Mid-Continent.

Padgett, P., 1988, Petrology, diagenesis and depositional environment of the Tonkawa Sandstone in southwestern Dewey County, Oklahoma: Oklahoma State University, Master's Thesis.

Off, T., 1963, Rhythmic linear sand bodies caused by tidal currents: American Association of Petroleum Geologists Bulletin, v. 47, no. 2, p. 324-341.

Olariu, M. I., Carvajal, C. R., Olariu, C., and Steel, R. J., 2012, Deltaic process and architectural evolution during cross-shelf transits, Maastrichtian Fox Hills Formation, Washakie Basin, Wyoming. AAPG bulletin, 96(10), 1931-1956.

Pate, J.D., 1959, Stratigraphic traps along the north shelf of the Anadarko Basin, Oklahoma: AAPG Bulletin, v. 34, p. 39-59.

Rascoe, B., Jr., 1962, Regional stratigraphic analysis of Pennsylvanian and Permian rocks in western mid-continent: Colorado, Kansas, Oklahoma, Texas; AAPG Bulletin, v. 46, no. 8, p. 1357-1370.

Reineck, H. E., and Singh, I. B., 1973, Depositional sedimentary environments: with reference to terrigenous clastics: Berlin, Springer-Verlag, 439 p.

Reineck, H. E., and Wunderlich, F., 1968, Classification and origin of flaser and lenticular bedding: Sedimentology, V. 11, p. 99-1 04.

Reinson, G. E., Clark, J. E., and Foscolos, A. E., 1988, Reservoir geology of Crystal-Viking field, Lower Cretaceous estuarine tidal channel-bay complex, South-Central Alberta: American Association of Petroleum Geologists Bulletin, v. 72, no. 10, p. 1270-1 294.

Van der Plas, L., and Tobi, A.C., 1965, A chart for judging the reliability of point counting results. ln. J Sci., 263, 87-90.

Van Wagoner, J. C., Mitchum, R. M., Campion, K. M., and Rahmanian, V. D. 1990, Siliciclastic sequence stratigraphy in well logs, cores, and outcrops: American Association of Petroleum Geologists, Methods in Exploration Series, v. 7, p. 1–55.

Van Wagoner, J. C., Posamentier, H. W., Mitchum, R.M., Vail, P.R., Sarg, J.F., Loutit, T.S., and Hardenbol, J., 1988, An overview of sequence stratigraphy and key definitions, in C. W. Wilgus et al., eds., Sea level changes: an integrated approach: Society of Economic Paleontologists and Mineralogists Special Publication 42, p.39-45.

Van Wagoner, J. C., Mitchum, R. M., Posamentier, H. W., and Vail, P. R., 1987, Seismic stratigraphy interpretation using sequence stratigraphy: Part 2: Key definitions of sequence stratigraphy, AAPG Studies in Geology #27, v. 1, p. 11-14

Visser, M. J. 1980, Neap-spring cycles reflected in Holocene subtidal large-scale bedform deposits: a preliminary note: Geology, v. 8, p. 543-546.

Vita

Logan Brien Tussey was born on September 5, 1990 to Michael G. Tussey and Kathy L. O'Brien in Richmond, Virginia. He graduated from Alamo Heights High School in San Antonio, Texas in 2008 and continued his education at Auburn University, in Auburn, Alabama where he received a B.S. in Geology in 2012. He began pursuing an M.S. in Energy and Earth Resources at the University of Texas at Austin in 2013.